Spring 5-6-2015

The Effect of Extended π-Conjugation on the Spectroscopic and Electrochemical Properties of Boron Difluoride Formazanate Complexes

Stephanie M. Barbon

Viktor N. Staroverov

Joe Gilroy
jgilroy5@uwo.ca

The Effect of Extended π-Conjugation on the Spectroscopic and Electrochemical Properties of Boron Difluoride Formazanate Complexes

*Stephanie M. Barbon, Viktor N. Staroverov and Joe B. Gilroy**

Department of Chemistry and the Centre for Advanced Materials and Biomaterials Research (CAMBR), The University of Western Ontario, 1151 Richmond St. N., London, Ontario, Canada, N6A 5B7. Tel: +1-519-661-2111 ext. 81561; E-mail: joe.gilroy@uwo.ca

TOC Graphic:

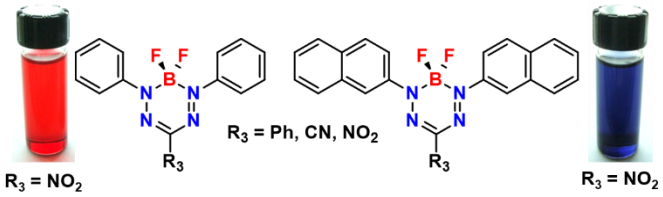

Abstract

The effect of extended π-conjugation on the spectroscopic and electrochemical properties of boron difluoride (BF_2) formazanate complexes was studied by the systematic comparison of phenyl- and naphthyl-substituted derivatives. Each of the BF_2 complexes described was characterized by ^{1}H, ^{13}C, ^{11}B and ^{19}F NMR spectroscopy, cyclic voltammetry, infrared spectroscopy, UV-vis absorption and emission spectroscopy and mass spectrometry. X-ray crystallography and electronic structure calculations were used to rationalize the trends observed, including direct comparison of 3-cyano-, 3-nitro- and 3-phenyl-substituted BF_2 formazanate complexes. In all cases, the wavelength of maximum absorption and emission were red-shifted as π-conjugation was systematically extended (by replacing phenyl with naphthyl), fluorescence quantum yields increased (up to tenfold) and electrochemical conversion of the formazanate complexes to their radical anion and dianion forms occurred at less negative potentials (easier to reduce).

Introduction

It has long been known that extended π-conjugation has a drastic effect on the electronic properties and spectroscopic features of molecules containing fused aromatic rings. Perhaps the simplest molecules that demonstrate this behavior are benzene, naphthalene and anthracene. In this series, as the extent of π-conjugation increases, the wavelength of maximum absorption, from ~260 nm for benzene, to ~310 nm for naphthalene and ~375 nm for anthracene, also increases.[1] The emission quantum yields of these compounds follow the same trend, increasing from 0.053 in benzene to 0.19 and 0.27 in naphthalene and anthracene, respectively.[1] As the structures of π-conjugated molecules become increasingly complex, so do their electronic properties, which often leads to their use in a variety of applications. π-Conjugated molecules are

frequently employed in photovoltaic cells,[2] as luminescent materials,[3] in field-effect transistors,[4] and as materials exhibiting aggregation-induced emission.[5]

Amongst the most common π-conjugated molecular materials are boron difluoride (BF_2) complexes of N,N-, O,O- and N,O-chelating ligands.[3,6] Boron dipyrromethenes (BODIPYs) are by far the most common of this class of complexes.[7,8] BODIPY **1**, which was first reported by Daub and coworkers in 1998, showed absorption and emission maxima around 500 nm, with an emission quantum yield of 0.60.[9] Ono *et al.* synthesized compound **2**, which is structurally very similar to **1**, but includes a greater degree of π-conjugation. The addition of two fused phenyl rings increased the wavelength of maximum absorption and emission by close to 100 nm, and the quantum yield to 0.91.[10] Similarly, Fu's group has applied this strategy to their naphthyridine BF_2 complexes **3**, **4**, and observed that by extending the conjugation of the naphthyridine ligand by a pyridine moiety, the solid-state fluorescence quantum yield increased by 0.20, and the wavelength of maximum absorption and emission was red-shifted by more than 20 nm.[11] Piers *et al.* have modified the structure of anilido-pyridine ligands to study the properties of the BF_2 complexes of both the parent anilido-pyridine complex **5** and the modified BF_2 complex **6**, which has a higher degree of π-conjugation. This modification nearly doubled the emission quantum yield from 0.33 to 0.60 and red-shifted the absorption and emission maxima by *ca.* 50 nm.[12]

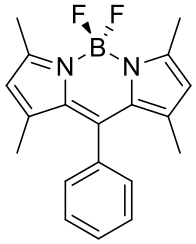

1

λ_{max} = 497 nm
λ_{em} = 505 nm
ϕ = 0.60

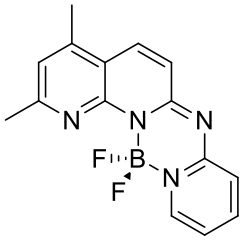

3

λ_{max} = 422 nm
λ_{em} = 527 nm
ϕ = 0.44

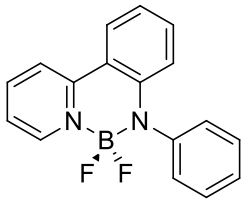

5

λ_{max} = 417 nm
λ_{em} = 531 nm
ϕ = 0.33

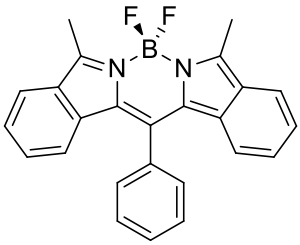

2

λ_{max} = 597 nm
λ_{em} = 606 nm
ϕ = 0.91

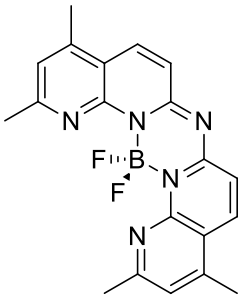

4

λ_{max} = 445 nm
λ_{em} = 557 nm
ϕ = 0.64

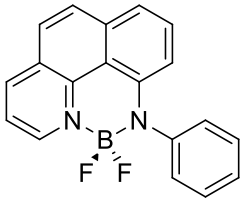

6

λ_{max} = 465 nm
λ_{em} = 584 nm
ϕ = 0.60

The Gilroy and Otten groups have recently shown that BF_2 complexes **7** derived from formazans[13] **8** have desirable spectroscopic and electrochemical properties that are easily tuned through structural variation.[14] In general, electron-withdrawing substituents were shown to increase reduction potentials (E^o_{red1} /E^o_{red2} become less negative) associated with radical anion and dianion formation and blue-shift the wavelength of maximum absorption and emission compared to phenyl-substituted analogs. Electron-donating substituents had the opposite effect, decreasing the reduction potentials (E^o_{red1} /E^o_{red2} become more negative), red-shifting the wavelength of maximum absorption and emission, and also increasing emission intensities. We have also recently demonstrated efficient electrochemiluminescence from a *p*-anisole-substituted boron difluoride formazanate complex (**7**: Ar_1 = Ar_5 = *p*-C_6H_4OMe, R_3 = CN).[15]

In an effort to assess the effect of extended π-conjugation on the properties of BF_2 formazanate dyes, and taking advantage of the ease of structural variation of the formazanate backbone, we have synthesized a series of formazans **8a−h** and BF_2 complexes **7a−h** by systematically introducing naphthyl (Np) substituents at the 1, 3 and 5 positions of the formazanate backbone.

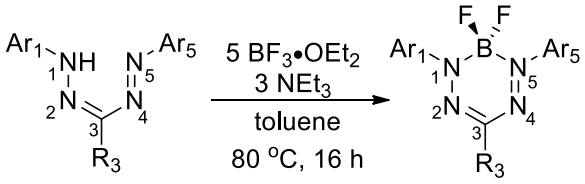

8 **7**

Scheme 1. Synthesis of BF_2 formazanate complexes.

Table 1. Substituents for formazans **8a−i** and BF_2 formazanate complexes **7a−i**.

	Ar_1	Ar_5	R_3
a	Ph	Ph	Ph
b	Ph	Ph	Np
c	Ph	Np	Ph
d	Np	Np	Ph
e[14b]	Ph	Ph	CN
f	Np	Np	CN
g	Ph	Ph	NO_2
h	Np	Np	NO_2
i[14a]	Ph	Ph	*p*-tolyl

Results and Discussion

Synthesis

Triarylformazans **8a−d**, 3-cyanoformazans **8e−f** and 3-nitroformazans **8g−h**, were synthesized by adapting previously published protocols.[16] Formazanate BF_2 complexes **7a−h** were prepared by refluxing the parent formazans in toluene in the presence of excess

triethylamine and boron trifluoride diethyl etherate (Scheme 1).[14b,14c] Analysis by ^{1}H, ^{11}B, ^{13}C and ^{19}F NMR spectroscopy (Figures S1–S24), mass spectrometry and IR spectroscopy confirmed the proposed structures of formazans **8a−h** and BF_2 complexes **7a−h**. The bidentate coordination mode observed for the formazanate ligands was consistent with other complexes of boron[14,17] and transition metals.[18]

Naphthyl-Substituted BF_2 Formazanate Complexes

By comparing 1,3,5-triphenyl-substituted BF_2 complex **7a** with naphthyl-substituted complexes **7b−d**, the effect of π-conjugation on the properties of BF_2 triarylformazanate complexes was explored. Molar absorptivities associated with π→π* transitions in **7a−d** ranged from 20,900 to 26,800 M^{-1} cm^{-1} in toluene. The replacement of one phenyl substituent for a naphthyl substituent in **7b** (Ar_1 = Ar_5 = Ph, R_3 = Np) and **7c** (Ar_1 = R_3 = Ph, Ar_5 = Np) caused a red shift of maximum absorption (λ_{max}) in toluene, from 517 nm for **7a** to 529 nm for **7b** and 535 nm for **7c**. The replacement of a second phenyl substituent in **7d** (Ar_1 = Ar_5 = Np, R_3 = Ph) resulted in a further red shift in λ_{max} to 556 nm (Figure 1a, S25, S26, Table 2). In order to verify that the observed absorption properties were not simply due to the presence of a naphthyl group, the UV-vis absorption spectrum of 2-naphthylamine was recorded (λ_{max} = 345 nm, Figure S27). Interestingly, when comparing compound **7b** and **7c**, which both have one naphthyl and two phenyl substituents, **7c** has a slightly longer wavelength of maximum absorption (529 vs. 535 nm).

All four compounds are weakly emissive, with maximum emission (λ_{em}) observed between 626 and 681 nm (Figures 1b, S25, S26, Table 2). The trend observed for the wavelengths of maximum absorption is mirrored here, with the λ_{em} of **7b−d** red-shifted with respect to **7a**. Quantum yields for all four complexes are below 0.05. However, the observed

Stokes shifts (ν_{ST}) were large (**7a**, ν_{ST} = 109 nm, 3368 cm^{-1}; **7b**, ν_{ST} = 124 nm, 3590 cm^{-1}; **7c**, ν_{ST} = 124 nm, 3517 cm^{-1}; **7d**, ν_{ST} = 125 nm, 3301 cm^{-1}).

Complexes **7a–d** (6 π electrons) are electrochemically active, exhibiting two reversible one-electron reduction waves corresponding to the reversible formation of ligand-centered radical anions (7 π electrons) and dianions (8 π electrons), respectively (Figure 2, Table 2). Closely related Kuhn-type verdazyls **9** and 6-oxoverdazyls **10** (7 π electrons), which also benefit from significant delocalization and stabilized frontier molecular orbitals due to the presence of four nitrogen atoms in their heterocyclic backbones, exhibit similar redox behavior and can be reversibly oxidized to cations (6 π electrons) and anions (8 π electrons).[16c] The reduction potentials observed for **7a–d** become less negative (easier to reduce) as naphthyl substituents are introduced (**7a**, −0.82 and −1.89 V; **7b**, −0.81 and −1.88 V; **7c**, −0.80 and −1.85 V; and **7d**, −0.78 and −1.78 V). This trend is consistent with naphthyl substituents having stabilized LUMOs due to enhanced π-conjugation when compared to phenyl substituents. A single naphthyl substituent at the 1,5-position has a more drastic effect than the same substituent at the 3 position, as **7c** is easier to reduce than **7b** by approximately 13 mV. Each complex also undergoes irreversible oxidation within the electrochemical window (Figure S28).

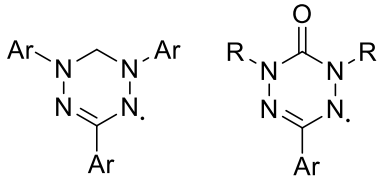

9 **10**

Ar = Ph, *p*-substituted Ph
R = Me, *i*Pr

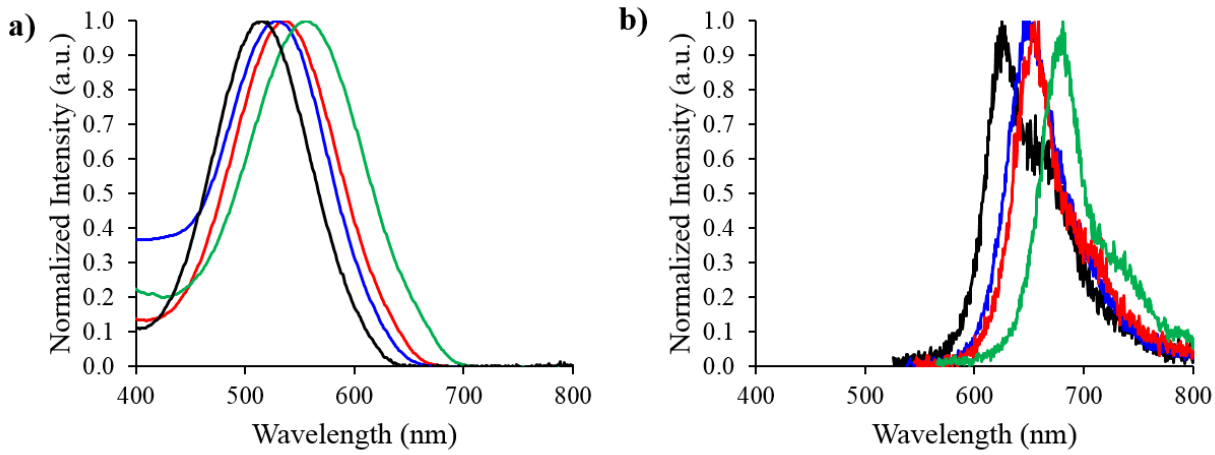

Figure 1. UV-vis absorption spectra (a) and emission spectra (b) of **7a** (black, $Ar_1 = Ar_5 = R_3 =$ Ph), **7b** (blue, $Ar_1 = Ar_5 =$ Ph, $R_3 =$ Np), **7c** (red, $Ar_1 = R_3 =$ Ph, $Ar_5 =$ Np) and **7d** (green, $Ar_1 = Ar_5 =$ Np, $R_3 =$ Ph) recorded for 10^{-5} M degassed toluene solutions.

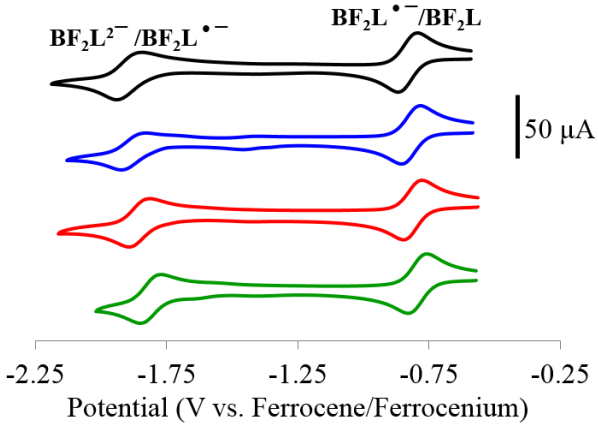

Figure 2. Cyclic voltammograms of **7a** (black, $Ar_1 = Ar_5 = R_3 =$ Ph), **7b** (blue, $Ar_1 = Ar_5 =$ Ph, $R_3 =$ Np), **7c** (red, $Ar_1 = R_3 =$ Ph, $Ar_5 =$ Np) and **7d** (green, $Ar_1 = Ar_5 =$ Np, $R_3 =$ Ph), recorded at 100 mV s^{-1} in 1 mM acetonitrile solutions containing 0.1 M tetrabutylammonium hexafluorophosphate as supporting electrolyte. L = redox-active formazanate ligand.

The data collected for compounds **7a–d** allows for the conclusion that extended π-conjugation has a dramatic effect on the properties of BF_2 formazanate complexes. Systematically extending π-conjugation increases the emission quantum yields, red-shifts the wavelengths of maximum absorption and emission, and raises the reduction potentials of the

resulting compounds. It is noteworthy that these data also demonstrate that extending the π-conjugation at the 3 position of the formazanate backbone has a less pronounced effect than similar structural modification at the 1,5-positions (see below).

Table 2. Solution characterization data for BF_2 complexes **7a**−**h**.

	Solvent	λ_{max} (nm)	ε (M^{-1} cm^{-1})	λ_{em} (nm)	Φ_f [a]	ν_{ST} (nm)	ν_{ST} (cm^{-1})	E^o_{red1} [b] (V)	E^o_{red2} [b] (V)
	THF	509	22,500	627	0.01	118	3697		
7a	toluene	517	23,800	626	< 0.01	109	3368	−0.82	−1.89
	CH_2Cl_2	509	23,400	630	0.01	121	3773		
	THF	522	22,000	658	0.01	136	3960		
7b	toluene	529	20,900	653	< 0.01	124	3590	−0.81	−1.88
	CH_2Cl_2	524	20,300	656	0.09	132	3840		
	THF	529	25,000	655	< 0.01	126	3636		
7c	toluene	535	26,800	659	0.02	124	3517	−0.80	−1.85
	CH_2Cl_2	530	27,500	656	0.03	126	3624		
	THF	550	22,900	680	0.02	130	3476		
7d	toluene	556	25,200	681	0.05	125	3301	−0.78	−1.78
	CH_2Cl_2	551	23,600	682	< 0.01	131	3486		
	THF	489	25,400	585	0.05	96	3356		
7e[14b]	toluene	502	30,400	586	0.15	84	2855	−0.53	−1.68
	CH_2Cl_2	491	34,600	584	0.09	93	3243		
	THF	551	27,700	676	0.25	125	3356		
7f	toluene	581	25,700	670	0.39	89	2286	−0.49	−1.54
	CH_2Cl_2	558	23,900	669	0.32	111	2973		
	THF	487	21,000	585	0.03	98	3440		
7g	toluene	505	26,000	590	0.05	85	2853	−0.48	−1.61
	CH_2Cl_2	488	29,200	587	0.03	99	3456		
	THF	561	27,500	679	0.23	118	3098		
7h	toluene	583	24,100	671	0.48	88	2250	−0.45	−1.49
	CH_2Cl_2	563	26,700	677	0.28	114	2991		

[a]Quantum yields were measured according to a previously reported method[19] using ruthenium tris(bipyridine) hexafluorophosphate as a relative standard,[20] and corrected for detector non-linearity (Figure S29). [b]Cyclic voltammetry experiments were conducted in acetonitrile containing 1 mM analyte and 0.1 M tetrabutylammonium hexafluorophosphate at a scan rate of 100 mV s^{-1}. All voltammograms were referenced internally against the ferrocene/ferrocenium redox couple.

3-Phenyl-, 3-Cyano- and 3-Nitro-Substituted BF_2 Formazanate Complexes

The influence of cyano-, nitro- and phenyl-substituents at the R_3 position of the formazanate backbone on the properties of BF_2 formazanate dyes was assessed through comparison of 1,5-diphenyl-substituted compounds **7a** (R_3 = Ph), **7e** (R_3 = CN) and **7g** (R_3 = NO_2). Single crystals of complex **7g** were grown by slow evaporation of a concentrated dichloromethane solution (Figure 3). The solid-state structure of complex **7e** has previously been published.[14b] Attempts to crystallize complex **7a** under a variety of conditions consistently resulted in weakly diffracting, multiply twinned crystals (likely due to the *pseudo* three-fold symmetry of **7a**) unsuitable for X-ray diffraction studies. Therefore, complex **7i** (Ar_1 = Ar_5 = Ph, R_3 = *p*-tolyl), previously reported by the Otten group,[14a] has been included for comparison as the structural metrics associated with the presence of a single *p*-tolyl substituent are not expected to differ significantly from those expected for complex **7a**. All three BF_2 complexes contain a four-coordinate boron center in a distorted tetrahedral geometry, which is slightly displaced from the plane of the formazanate backbone (-N=N-C=N-N-). It is also noteworthy that the formazanate backbone is delocalized in all three examples (Table 3) with the CN and NN bond lengths falling between typical single and double bonds for the respective atoms involved.[21] Each complex possesses moderate degrees of twisting between the *N*-aryl substituents and the formazanate backbone (**7e**, 22.0° and 24.4°, **7g**, 36.4° and 38.2° and **7i**, 48.0° and 42.0°). Overall we can conclude that structurally, all three complexes are very similar, and the nature of the R_3 substituent has little influence over the bond lengths and angles of the BF_2 formazanate heterocycle (Table 3).

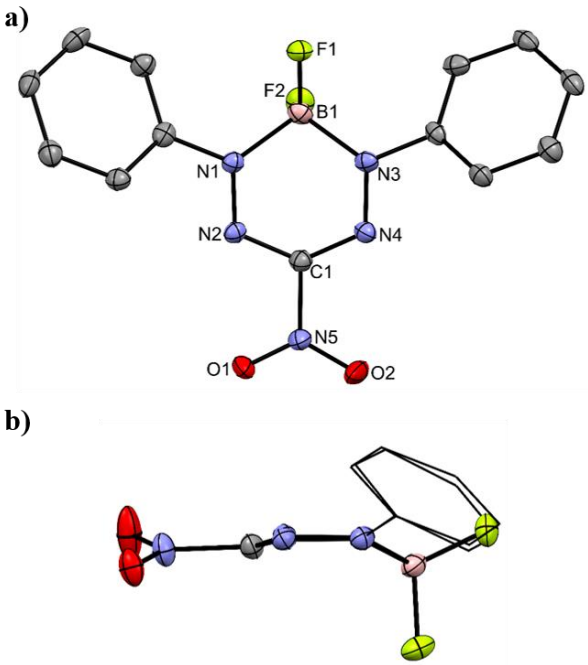

Figure 3. a) Top view and b) side view of the solid-state structure of BF_2 formazanate complex **7g**. Thermal ellipsoids are shown at 50% probability and hydrogen atoms have been removed for clarity. Only one of two structurally similar molecules in the asymmetric unit for **7g** is shown.

Table 3. Selected bond lengths (Å) and angles (degrees) for BF_2 formazanate complexes **7e**, **7g** and **7i**,[14a] determined by single crystal X-ray diffraction.

	7e	**7g**[a]	**7i**[b,14a]
N1-N2, N3-N4	1.2900(15), 1.2948(15)	1.302(5), 1.304(5)	1.308(1), 1.308(1)
C1-N2, C1-N4	1.3408(17), 1.3379(17)	1.330(5), 1.318(5)	1.346(1), 1.343(1)
N1-B1, N3-B1	1.5748(18), 1.5771(17)	1.576(6), 1.563(6)	1.559(2), 1.552(2)
N1-B1-N3	105.55(10)	103.4(3)	102.40(9)
N2-N1-B1, N4-N3-B1	124.78(10), 124.32(11)	121.5(3), 122.2(3)	121.45(9), 121.69(9)
N2-C1-N4	129.33(12)	130.0(4)	124.2(1)
C1-N2-N1, C1-N4-N3	117.14(11), 117.30(11)	115.6(3), 115.5(3)	117.68(9), 117.72(9)
Boron displacement[c]	0.192	0.456	0.500
Dihedral angles[d]	18.7, 26.2	36.4, 38.2	48.0, 42.0

[a] The second molecule in the unit cell of **7g** has very similar structural metrics. [b]The numbering convention for the structure previously reported by Otten and co-workers[14a] has been modified for ease of comparison. [c]Distance between B1 and N_4 plane. [d]Angles between the plane defined by the N1 and N3 aryl substituents and the N_4 plane.

As both cyano and nitro groups are strongly electron-withdrawing, complexes **7e** and **7g** have similar spectroscopic and electrochemical properties, though they differ significantly when compared to complex **7a**. All three complexes are strongly absorbing between 400 and 600 nm

($\pi \rightarrow \pi^*$), though their λ_{max} range from 502 nm (**7e**) to 505 nm (**7g**) and 517 nm (**7a**) (Figures 4a, S30, S31, Table 2). Time-dependent DFT studies have confirmed the HOMO and LUMO to be the dominant orbital pair involved for the lowest energy transition in complexes **7a**, **7e**, **7g** (see below, Table 4). While all three phenyl-substituted complexes are fluorescent (Figure 4b, Table 2), their emission quantum yields in toluene vary dramatically (**7a**: λ_{em} = 626 nm, Φ = <0.01, **7e**: λ_{em} = 586 nm, Φ = 0.15, **7g**: λ_{em} = 590 nm, Φ = 0.05). We assume that the difference in quantum yields is likely due to non-radiative decay pathways associated with the 3-phenyl substituent. While complex **7a** has the lowest quantum yield, it has the largest Stokes shift (ν_{ST} = 109 nm, 3368 cm^{-1}) in toluene, significantly higher than complexes **7e** (ν_{ST} = 84 nm, 2855 cm^{-1}) and **7g** (ν_{ST} = 85 nm, 2853 cm^{-1}). Given the qualitative similarities of the emission spectra in different solvents (Figures S25, S26, S30 and S31), we believe that the low-energy shoulders observed can be attributed to vibrational overtones rather than aggregation.

Finally, the electron-withdrawing nature of the R_3 substituent has a significant effect on the electrochemical properties of BF_2 formazanate complexes. Complex **7g** (R_3 = NO_2) is the easiest to reduce, with the first and second one-electron reductions occurring at −0.48 V and −1.61 V vs. ferrocene/ferrocenium. Complex **7e** (R_3 = CN) is slightly more difficult to reduce at potentials of −0.53 V and −1.68 V. Finally, complex **7a** (R_3 = Ph), is substantially more difficult to reduce, with the sequential one-electron reductions occurring at −0.82 V and −1.89 V (Figure S32, Table 2).

As mentioned earlier, the properties of complexes bearing phenyl and naphthyl substituents at the 3-position of the formazanate backbone did not differ dramatically. We have also previously shown that the substitution of electron-donating and withdrawing groups introduced on aryl rings at the 3-position of the formazanate backbone did not significantly alter

the properties of the resulting BF_2 complexes.[14c] However, complexes **7a**, **7e** and **7g** clearly demonstrate that the same trend is not true for all substituents at the 3 position, as the properties of **7e** (R_3 = CN) and **7g** (R_3 = NO_2) are drastically different than those of **7a** (R_3 = Ph). This is likely due to the strong electron-withdrawing characteristics of the cyano and nitro substituents, and less related to the extent of π-conjugation in these complexes.

By comparing naphthyl-substituted complexes **7d**, **7f** and **7h**, with phenyl-substituted complexes **7a**, **7e** and **7g**, the effect of π-conjugation on the properties of BF_2 3-phenyl-, 3-cyano- and 3-nitro-formazanate complexes was studied. The wavelength of maximum absorption of naphthyl substituted complexes **7d**, **7f** and **7h** were red-shifted (relative to the phenyl-substituted analogs **7a**, **7e** and **7g**), from 502 to 581 nm for complex **7f** (R_3 = CN), from 505 to 583 nm for complex **7h** (R_3 = NO_2) and from 517 to 556 nm for complex **7d** (R_3 = Ph) (Figure 4c, Table 2). While in all three cases the observed trend was the same, the magnitude of the red-shift upon replacement of two phenyl substituents with two naphthyl substituents was much greater for complexes with strongly electron withdrawing R_3 substituents [$\Delta\lambda_{max}$ = 79 nm, 2709 cm^{-1} (R_3 = CN); $\Delta\lambda_{max}$ = 78 nm, 2649 cm^{-1} (R_3 = NO_2); $\Delta\lambda_{max}$ = 39 nm, 1357 cm^{-1} (R_3 = Ph)].

The emission spectra of complexes **7d**, **7f** and **7h** (Figure 4d, Table 2) were also red-shifted with respect to the phenyl-substituted analogs, with λ_{em} of 681 nm (**7d**), 670 nm (**7f**) and 671 nm (**7g**) in toluene. The emission quantum yields of these three complexes were significantly higher than the quantum yields of the phenyl-substituted complexes. The addition of the naphthyl substituent increases the emission quantum yield for **7d** to 0.05 (from < 0.01 in complex **7a**), for **7f** to 0.39 (from 0.15 in complex **7e**) and for **7h** to 0.48 (from 0.05 in complex **7g**). The Stokes shifts observed for the 3-cyano- and 3-nitro-substituted complexes were smaller than those of 3-phenyl substituted complexes. All complexes with R_3 = cyano or nitro have

Stokes shifts ranging from 84 to 89 nm (2250–2855 cm^{-1}) in toluene, while those with R_3 = Ph, have generally larger Stokes shifts, from 109−125 nm (3368–3590 cm^{-1}) in toluene.

The cyclic voltammograms of complexes **7d**, **7f** and **7h** demonstrate that the more electron-deficient complexes **7f** and **7h** are significantly easier to reduce (by almost 0.300 V) than complex **7d** (Figure 5, Table 2). In all three examples, the reduction potential of the naphthyl-substituted complexes was 0.030–0.045 V higher than the phenyl-substituted analogs. Complexes **7f**, **7g** and **7h** also underwent irreversible oxidation within the electrochemical window of the solvent (CH_3CN) (Figure S33).

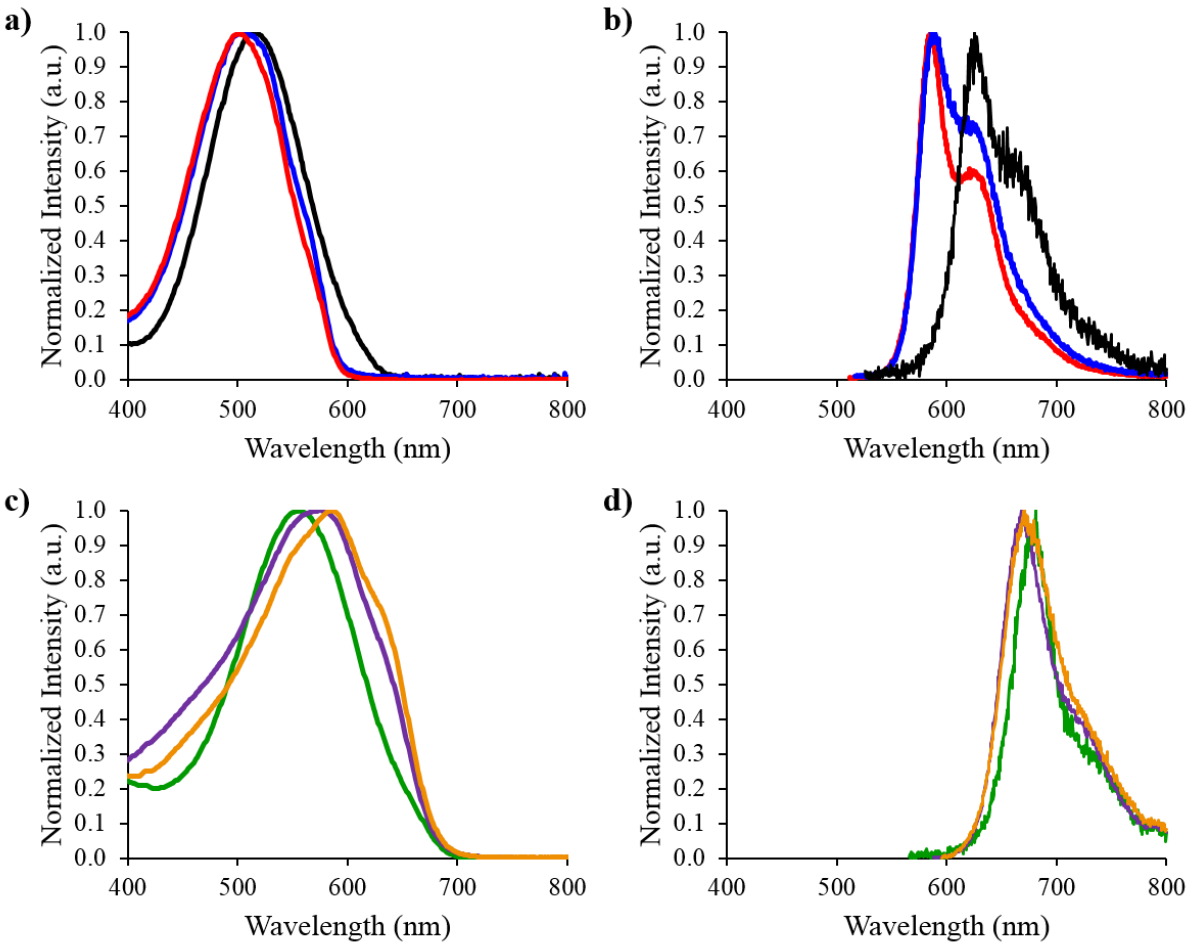

Figure 4. UV-vis absorption spectra (a) and emission spectra (b) of **7a** (black, Ar_1 = Ar_5 = R_3 = Ph), **7e** (red, Ar_1 = Ar_5 = Ph, R_3 = CN) and **7g** (blue, Ar_1 = Ar_5 = Ph, R_3 = NO_2). UV-vis absorption spectra (c) and emission spectra (d) of **7d** (green, Ar_1 = Ar_5 = Np, R_3 = Ph), **7f** (purple, Ar_1 = Ar_5 = Np, R_3 = CN) and **7h** (orange, Ar_1 = Ar_5 = Np, R_3 = NO_2) recorded for 10^{-5} M degassed toluene solutions.

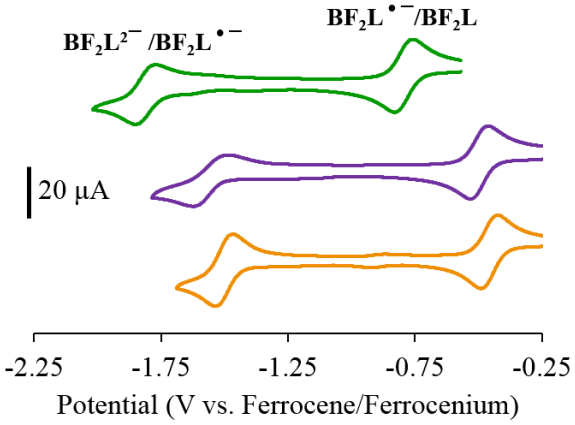

Figure 5. Cyclic voltammograms of **7d** (green, $Ar_1 = Ar_5 = Np$, $R_3 = Ph$), **7f** (purple, $Ar_1 = Ar_5 = Np$, $R_3 = CN$) and **7h** (orange, $Ar_1 = Ar_5 = Np$, $R_3 = NO_2$). Cyclic voltammograms were recorded at 100 mV s^{-1} in 1 mM acetonitrile solutions containing 0.1 M tetrabutylammonium hexafluorophosphate as supporting electrolyte.

Electronic Structure Calculations

In an attempt to rationalize the trends observed, we calculated the highest occupied and lowest unoccupied molecular orbitals (HOMOs and LUMOs) of **7a**, **7e** and **7g** (Figure 6 and Table 4) with the *Gaussian 09* program[22] using the M06 density functional[23] and the 6-311+G* basis set, in vacuum and in toluene solution. The Kohn–Sham molecular orbitals of **7a**, **7e** and **7g** were computed for the corresponding optimized molecular structures. The UltraFine integration grid was employed in all calculations. Solvation effects were treated implicitly using the polarizable continuum model (SCRF=PCM). All optimized structures of **7a**, **7e** and **7g** have C_s symmetry and were confirmed by vibrational analysis to be minima on the potential energy surface, both in vacuum and in toluene solution (see ESI for further details).

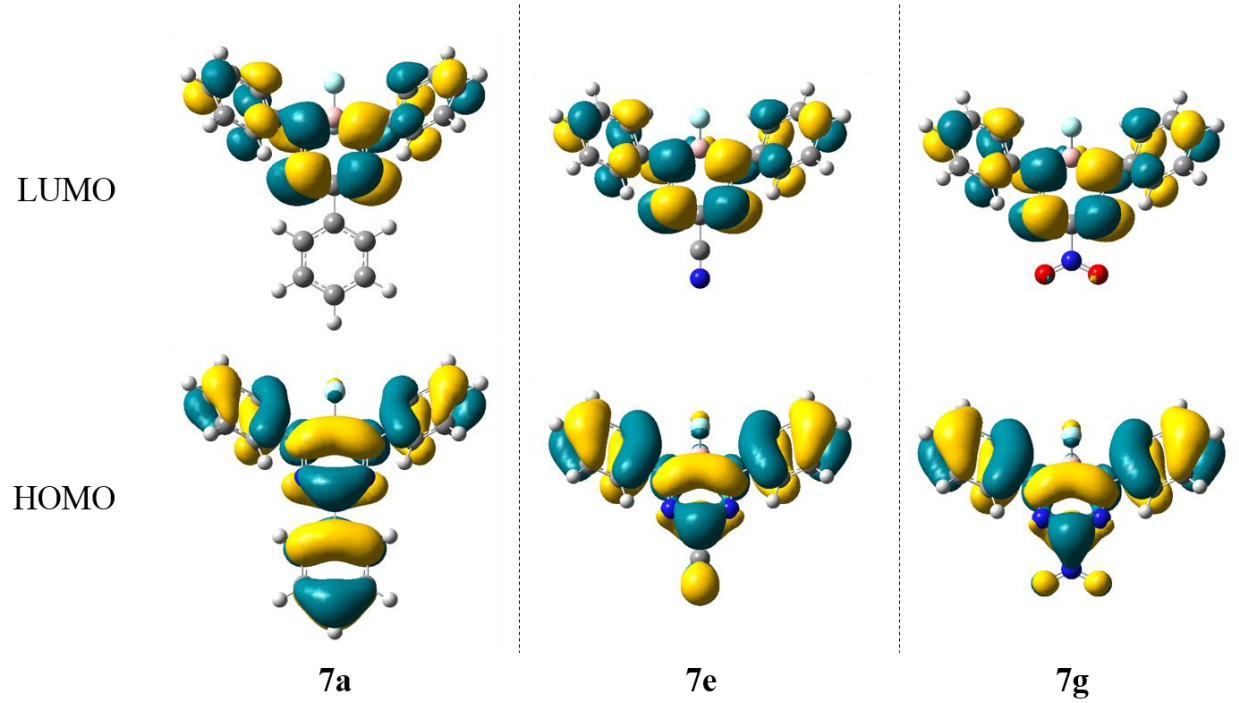

Figure 6. HOMOs and LUMOs for BF_2 complexes **7a** (Ar_1 = Ar_5 = R_3 = Ph), **7e** (Ar_1 = Ar_5 = Ph, R_3 = CN) and **7g** (Ar_1 = Ar_5 = Ph, R_3 = NO_2) calculated in toluene solution.

Table 4. HOMO/LUMO energies for BF_2 complexes **7a** (Ar_1 = Ar_5 = R_3 = Ph), **7e** (Ar_1 = Ar_5 = Ph, R_3 = CN) and **7g** (Ar_1 = Ar_5 = Ph, R_3 = NO_2) in vacuum and toluene solution calculated at the M06/6–311+G* level of theory using the SCRF method.

Compound	Lowest Excitation Energy[a]		ε_{HOMO} (eV)	ε_{LUMO} (eV)	HOMO-LUMO Gap	
	(eV)	(nm)			(eV)	(nm)
Vacuum						
7a	2.56	484	–6.38	–3.25	3.13	397
7e[14b]	2.76	448	–7.12	–3.79	3.34	372
7g	2.79	444	–7.24	–3.85	3.39	366
Toluene Solution						
7a	2.50	496	–6.45	–3.30	3.15	393
7e[14b]	2.65	468	–7.12	–3.76	3.36	369
7g	2.67	464	–7.23	–3.83	3.40	365

[a]Computed using time-dependent DFT.

The calculated LUMOs for complexes **7a**, **7e** and **7g** are highly delocalized over the formazanate backbone and *N*-aryl substituents, but do not extend over the 3-substituents. By

contrast, the HOMOs are delocalized over both the *N*-aryl and 3-substituents (Ph, CN and NO_2). The electrochemical reduction of complexes **7a**, **7e** and **7g** should primarily involve the LUMOs of each complex. Based solely on the shape of the calculated frontier orbitals, the reduction potentials for each compound should be similar. However, due to the differing electron-withdrawing characteristics of the 3-subsitutents, the experimentally determined reduction potentials varied significantly. The observed trend in the first and second reduction potentials (E^o_{red1} and E^o_{red2}), which involves stepwise population of the LUMO, was consistent with the trend in computed LUMO energies (ε_{LUMO}) in toluene solution: **7g** (–3.83 eV) < **7e** (–3.76 eV) < **7a** (–3.30 eV). The finding that the LUMOs do not extend over the 3-substituent is also consistent with the fact that the reduction potentials observed for 1,5-diphenyl-substituted complexes **7a** (R_3 = Ph) and **7b** (R_3 = Np) are similar. The small difference in these potentials may be attributed to the subtle difference in the electron-withdrawing nature of phenyl and naphthyl substituents.

The absorption and emission properties of BF_2 formazanate complexes **7a**, **7e** and **7g** varied significantly, and involve both the HOMO and LUMO orbitals. While both the HOMO/LUMO for **7a** were significantly higher in energy than those found for complexes **7e** and **7g**, destabilization of the HOMO, due to the extended π-conjugation associated with the 3-phenyl substituent, is the dominating factor that leads to red-shifting of its absorption and emission spectra relative to **7e** and **7g**. Although one cannot expect quantitative agreement between HOMO-LUMO gaps and lowest electronic excitation energies, we note that the observed trends in λ_{max} and λ_{em} are consistent with the trends in calculated HOMO-LUMO gaps in toluene [**7a** (393 nm) > **7e** (369 nm) ≈ **7g** (365 nm)].

Conclusion

In conclusion, we have described the synthesis and characterization of eight BF_2 formazanate complexes allowing us to systematically assess the effect of extended π-conjugation on the spectroscopic and electrochemical properties of BF_2 formazanate complexes. In general, extending the π-conjugation of complexes by replacing phenyl substituents with naphthyl substituents increased fluorescence quantum yields, increased (less negative) reduction potentials and red-shifted the wavelengths of maximum absorption and emission. We have also demonstrated the differences in properties between BF_2 complexes of 3-aryl-, cyano- and nitro-formazans relate primarily to the electron-withdrawing nature of the 3-substituents (NO_2 > CN >> Ph). The complexes of 3-cyano and 3-nitro formazans have significantly increased emission quantum yields, and their properties are very sensitive to extension of their π-systems. Our future work in this area will focus on the incorporation of BF_2 formazanate complexes into functional polymers with further extended π-conjugation.

Experimental Section

General Considerations

All reactions and manipulations were carried out under a nitrogen atmosphere using standard Schlenk techniques unless otherwise stated. Solvents were obtained from commercial sources, purified using a standard solvent purification system, collected under vacuum and stored under a nitrogen atmosphere over 4 Å molecular sieves. The synthesis and characterization of formazans **8a**,[16c] **8e** and **8g**,[16d] and BF_2 complex **7e**[14b] have been reported previously. All other reagents were purchased from commercial sources and used as received.

NMR Spectra were recorded on a 400 MHz (^{1}H: 399.8 MHz, ^{11}B: 128.3 MHz, ^{19}F: 376.1 MHz) or 600 MHz (^{1}H: 599.5 MHz, ^{13}C: 150.8 MHz) spectrometer. ^{1}H NMR spectra were

referenced to residual $CHCl_3$ (7.26 ppm) or DMSO-d_5 (2.50 ppm) and ^{13}C NMR spectra were referenced to $CDCl_3$ (77.2 ppm), CD_2Cl_2 (53.8 ppm) or DMSO-d_6 (39.5 ppm). ^{11}B spectra were referenced to $BF_3{\cdot}OEt_2$ at 0 ppm and ^{19}F spectra were referenced to $CFCl_3$ at 0 ppm. Mass spectrometry data were recorded in positive-ion mode using electron impact ionization and electrospray ionization. UV-vis absorption data was obtained by running four separate concentrations for each sample and molar extinction coefficients were determined from the slope of a plot of absorbance against concentration. Infrared spectra were recorded on a KBr disk. Fluorescence spectra were collected for degassed solutions using a commercial spectrophotometer. Excitation wavelengths for the emission spectra were chosen based on λ_{max} from the respective UV-vis absorption spectrum in the same solvent. Quantum yields were estimated relative to ruthenium tris(bipyridine) hexafluorophosphate by previously described methods and corrected for wavelength dependent detector sensitivity (Figure S29).[19-20]

Electrochemical Methods

Cyclic voltammograms were recorded using a commercially available potentiostat. Electrochemical cells consisted of a three-electrode setup including a glassy carbon working electrode, platinum wire counter electrode and silver wire *pseudo* reference electrode. Experiments were run at scan rates of 100 mV s^{-1} in degassed acetonitrile solutions of the analyte (~1 mM) and supporting electrolyte (0.1 M tetrabutylammonium hexafluorophosphate). Cyclic voltammograms were referenced against an internal standard (~1 mM ferrocene) and corrected for internal cell resistance using commercial software.

X-ray Crystallography Details

Single crystals of complex **7g** suitable for X-ray diffraction studies was grown by slow evaporation of a concentrated dichloromethane solution. The sample was mounted on a Mitegen

polyimide micromount with a small amount of Paratone N oil. All X-ray measurements were made at a temperature of 110 K. The data collection strategy included a number of ω and φ scans which collected data over a range of angles, 2θ. The frame integration was performed using SAINT.[24] The resulting raw data was scaled and absorption corrected using a multi-scan averaging of symmetry equivalent data using SADABS.[25] The structures were solved by direct methods using the XS program.[26] All non-hydrogen atoms were obtained from the initial solution. The hydrogen atoms were introduced at idealized positions and were allowed to refine isotropically. The structural model was fit to the data using full matrix least-squares based on F^2. The calculated structure factors included corrections for anomalous dispersion from the usual tabulation. The structure was refined using the SHELXL-2014 program from SHELXTL.[27] See Table 5 for additional crystallographic data.

Table 5. X-ray diffraction data collection and refinement details for BF_2 complex **7g**.

	7g
Chemical Formula	$C_{13}H_{10}BF_2N_5O_2 \cdot C_{0.50}HCl$
FW (g/mol)	359.53
Crystal Habit	red prism
Crystal System	monoclinic
Space Group	P 2_1/n
T (K)	110
λ (Å)	0.71073
a (Å)	9.555(8)
b (Å)	17.226(11)
c (Å)	18.840(14)
α (deg)	90
β (deg)	98.070(13)
γ (deg)	90
V (Å^3)	3070(4)
Z	8
ρ (g/cm^3)	1.556
μ (cm^{-1})	0.290
R_1,[a] wR_2[b] [I > 2σ]	0.0588, 0.1730
R_1, wR_2 (all data)	0.0811, 0.1901
GOF[c]	1.025

[a] $R_1 = \Sigma(|F_o| - |F_c|) / \Sigma F_o$, [b] $wR_2 = [\Sigma(w(F_o^2 - F_c^2)^2) / \Sigma(w F_o^4)]^{½}$, [c] GOF = $[\Sigma(w(F_o^2 - F_c^2)^2) /$ (No. of reflns. - No. of params.) $]^{½}$

Representative procedure for the preparation of formazans 8b and 8c:

Formazan 8b (Ar_1 = Ar_5 = Ph, R_3 = Np)

In air, phenyl hydrazine (0.69 g, 0.63 mL, 6.4 mmol) was dissolved in ethanol (15 mL). 2-Naphthylaldehyde (1.00 g, 6.40 mmol) was then added and the solution was allowed to stir for 10 min. After this time, a light yellow precipitate had formed. Dichloromethane (50 mL) and water (50 mL) were added to form a biphasic reaction mixture. Sodium carbonate (2.17 g, 20.5 mmol) and tetrabutyl ammonium bromide (0.21 g, 0.64 mmol) were added and the mixture was cooled in an ice bath to 0 °C. In a separate flask, aniline (0.60 g, 6.4 mmol) and concentrated hydrochloric acid (1.6 mL) were mixed in water (15 mL) and cooled in an ice bath. A cooled

solution of sodium nitrite (0.51 g, 7.4 mmol) in water (5 mL) was added slowly to the amine solution. This mixture was left to stir at 0 °C for 30 min, after which time it was added dropwise to the biphasic reaction mixture described above over 10 min. The resulting solution was stirred for 18 h, which gradually turned dark red over this time. The dark red organic fraction was then washed with deionized water (3 x 50 mL), dried over $MgSO_4$, gravity filtered and concentrated *in vacuo*. The resulting residue was purified by flash chromatography (dichloromethane, neutral alumina) to afford formazan **8b** as a dark red microcrystalline solid. Yield = 1.11 g, 50%. Melting point = 124–126 °C. ^{1}H NMR (599.5 MHz, $CDCl_3$) δ 15.49 (s, 1H), 8.62 (s, 1H), 8.29–8.28 (m, 1H), 7.95–7.87 (m, 3H), 7.74 (d, $^3J_{HH}$ = 8 Hz, 4H), 7.52–7.48 (m, 6H), 7.33–7.30 (m, 2H). ^{13}C{^{1}H} NMR (100.6 MHz, $CDCl_3$): δ 148.0, 141.1, 135.0, 133.7, 133.1, 129.5, 128.6, 128.0, 127.7, 127.6, 126.1, 125.9, 124.7, 124.1, 118.9. FT-IR (KBr): 3267 (br, s), 3055 (s), 026 (m), 2915 (m), 2846 (m), 1598 (s), 1501 (s), 1453 (m), 1348 (m), 1253 (s), 1226 (s) cm^{-1}. UV-vis (toluene): λ_{max} = 498 nm (ε = 10, 100 M^{-1} cm^{-1}). Mass Spec. (EI, +ve mode): exact mass calculated for $[C_{23}H_{18}N_4]^+$: 350.1532; exact mass found: 350.1537; difference: +1.6 ppm.

Formazan 8c (Ar_1 = R_3 = Ph, Ar_5 = Np)

In air, from 6.98 mmol of hydrazine/aldehyde: Yield = 2.24 g, 92%. Melting point = 140–142 °C. ^{1}H NMR (400.1 MHz, $CDCl_3$) δ 15.56 (s, 1H), 8.21 (d, $^3J_{HH}$ = 7 Hz, 2H), 8.04 (s, 1H), 7.93–7.88 (m, 3H), 7.85–7.83 (m, 1H), 7.69 (d, $^3J_{HH}$ = 8 Hz, 2H), 7.56–7.47 (m, 6H), 7.43–7.40 (m, 1H), 7.31–7.28 (m, 1H). ^{13}C{^{1}H} NMR (100.6 MHz, $CDCl_3$): δ 147.4, 146.4, 141.4, 137.6, 134.0, 133.3, 129.6, 129.5, 128.5, 128.5, 128.1, 127.8, 127.1, 127.0, 126.5, 126.0, 120.1, 118.5, 116.5. FT-IR (KBr): 3242 (br, s), 3050 (m), 3021 (m), 2915 (m), 2847 (m), 1597 (m), 1515 (m), 1494 (s), 1445 (m), 1348 (m), 1227 (s) cm^{-1}. UV-vis (toluene): λ_{max} = 508 nm (ε = 16, 500 M^{-1}

cm^{-1}). Mass Spec. (EI, +ve mode): exact mass calculated for $[C_{23}H_{18}N_4]^+$: 350.1532; exact mass found: 350.1537; difference: +1.6 ppm.

Preparation of formazan 8d (Ar_1 = Ar_5 = Np, R_3 = Ph)

In air, phenylpyruvic acid (0.51 g, 3.1 mmol) was dissolved in 150 mL deionized water with sodium hydroxide (0.94 g, 23 mmol) and cooled in an ice bath for 30 min. In a separate flask, 2-naphthylamine (1.00 g, 6.98 mmol) and concentrated hydrochloric acid (1.7 mL) were mixed in water (15 mL) and cooled in an ice bath for 10 min. A cooled solution of sodium nitrite (0.55 g, 8.0 mmol) in water (5 mL) was added slowly to the amine solution. This mixture was left to stir at 0 °C for 30 min, after which time it was added dropwise to the phenylpyruvic acid reaction mixture described above over a 10 min period. The resulting solution was stirred for 18 h, during which time a dark purple precipitate was formed. The dark purple solid was filtered off and purified by flash chromatography (dichloromethane, neutral alumina) to afford formazan **8d** as a dark purple microcrystalline solid. Yield = 1.03 g, 82%. Melting point = 152–154 °C. ^{1}H NMR (599.5 MHz, $CDCl_3$) δ 15.72 (s, 1H), 8.24 (d, $^3J_{HH}$ = 7 Hz, 2H), 8.12 (s, 2H), 7.97–7.91 (m, 6H), 7.87 (d, $^3J_{HH}$ = 8 Hz, 2H), 7.56–7.47 (m, 6H), 7.42–7.38 (m, 1H). ^{13}C{^{1}H} NMR (100.6 MHz, $CDCl_3$): δ 145.8, 141.8, 137.6, 134.1, 133.1, 129.7, 128.6, 128.4, 128.2, 127.9, 127.1, 126.3, 126.2, 119.1, 116.5. FT-IR (KBr): 3267 (br, s), 3050 (s), 3034 (m), 2914 (m), 2847 (m), 1629 (m), 1596 (s), 1499 (s), 1438 (m), 1358 (m), 1226 (s) cm^{-1}. UV-vis (toluene): λ_{max} = 532 nm (ε = 10, 300 M^{-1} cm^{-1}). Mass Spec. (EI, +ve mode): exact mass calculated for $[C_{27}H_{20}N_4]^+$: 400.1688; exact mass found: 400.1695; difference: +1.8 ppm.

Preparation of formazan 8f (Ar_1 = Ar_5 = Np, R_3 = CN)

In air, cyanoacetic acid (0.30 g, 3.5 mmol) was dissolved in 150 mL deionized water with sodium hydroxide (1.40 g, 34.9 mmol) and cooled in an ice bath. In a separate flask, 2-naphthylamine (1.00 g, 6.98 mmol) and concentrated hydrochloric acid (1.7 mL) were mixed in water (15 mL) and cooled in an ice bath. A cooled solution of sodium nitrite (0.55 g, 8.0 mmol) in water (5 mL) was added slowly to the amine solution. This mixture was left to stir at 0 °C for 30 min, after which time it was added dropwise to the cyanoacetic acid solution described above over a 10 min period. The resulting solution was stirred for 18 h, during which time a dark red precipitate was formed. The dark red solid was filtered off and purified by flash chromatography (dichloromethane, neutral alumina) to afford formazan **8f** as a dark red microcrystalline solid. Yield = 1.06 g, 86%. Melting point = 187–189 °C. ^{1}H NMR (599.5 MHz, DMSO-d_6) δ 12.90 (s, 1H), 8.39 (s, 2H), 8.18−7.88 (m, 8H), 7.62−7.51 (m, 4H). ^{13}C{^{1}H} NMR (100.6 MHz, DMSO-d_6): δ 144.9, 133.3, 132.7, 129.5, 128.6, 127.9, 127.8, 127.2, 127.0, 126.7, 116.5, 112.9. FT-IR (KBr): 3276 (br, m), 3053 (m), 2970 (m), 2219 (s), 1604 (s), 1531 (s), 1367 (m), 1346 (m), 1267 (m) cm^{-1}. UV-vis (toluene): λ_{max} = 472 nm (ε = 12, 900 M^{-1} cm^{-1}). Mass Spec. (EI, +ve mode): exact mass calculated for $[C_{22}H_{15}N_5]^+$: 349.1327; exact mass found: 349.1330; difference: +0.7 ppm.

Preparation of formazan 8h (Ar_1 = Ar_5 = Np, R_3 = NO_2)

In air, nitromethane (0.21 g, 0.19 mL, 3.5 mmol) was dissolved in 100 mL deionized water with sodium hydroxide (0.31 g, 7.7 mmol) and cooled in an ice bath. In a separate flask, 2-naphthylamine (1.00 g, 6.98 mmol) and concentrated hydrochloric acid (1.7 mL) were mixed in water (15 mL) and cooled in an ice bath. A cooled solution of sodium nitrite (0.55 g, 8.0 mmol) in water (5 mL) was added slowly to the amine solution. This mixture was left to stir at 0 °C for

30 min, after which time it was added dropwise to the nitromethane solution described above over a 10 min period. The resulting solution was stirred for 18 h, during which time a dark red precipitate was formed. The dark red solid was filtered off and purified by flash chromatography (dichloromethane, neutral alumina) to afford formazan **8h** as a dark red microcrystalline solid. Yield = 0.35 g, 27%. Melting point = 179–181 °C. ^{1}H NMR (599.5 MHz, $CDCl_3$) δ 15.63 (s, 1H), 8.18 (s, 2H), 8.00–7.96 (m, 6H), 7.90 (d, $^{3}J_{HH}$ = 7 Hz, 2H), 7.60–7.56 (m, 4H). $^{13}C\{^{1}H\}$ NMR (100.6 MHz, CD_2Cl_2): δ 144.5, 134.3, 133.9, 130.6, 129.1, 128.5, 127.9, 125.8, 122.0, 116.3, 110.4. FT-IR (KBr): 3242 (br, s), 3035 (m), 2915 (m), 2857 (m), 1589 (m), 1547 (s), 1502 (m), 1342 (s), 1277 (s) cm^{-1}. UV-vis (toluene): λ_{max} = 488 nm (ε = 12, 500 M^{-1} cm^{-1}). Mass Spec. (EI, +ve mode): exact mass calculated for $[C_{21}H_{15}N_5O_2]^{+}$: 369.1226; exact mass found: 369.1220; difference: −1.6 ppm. This compound decomposes over several hours in halogenated solvents.

Representative Procedure for the preparation of formazanate BF_2 complexes 7a-h:

Formazanate BF_2 Complex 7a (Ar_1 = R_3 = Ar_5 = Ph)

Formazan **8a** (0.50 g, 1.6 mmol) was dissolved in dry toluene (50 mL). Triethylamine (0.50 g, 0.68 mL, 4.9 mmol) was then added slowly and the solution was allowed to stir for 10 min. Boron trifluoride diethyl etherate (1.16 g, 1.01 mL, 8.15 mmol) was then added and the solution was heated at 80 °C for 18 h. The solution gradually turned from dark red to dark purple during this time. The reaction was then cooled to 20 °C and deionized water (10 mL) was added to quench any excess reactive boron-containing compounds. The red/purple toluene solution was then washed with deionized water (3 x 50 mL), dried over $MgSO_4$, gravity filtered and concentrated *in vacuo*. The resulting residue was purified by flash chromatography (dichloromethane, neutral alumina) to afford BF_2 complex **7a** as a dark purple microcrystalline

solid. Yield = 0.38 g, 67%. Melting point = 129–131 °C. ^{1}H NMR (599.5 MHz, $CDCl_3$) δ 8.12 (d, $^{3}J_{HH}$ = 7 Hz, 2H), 7.92 (d, $^{3}J_{HH}$ = 7 Hz, 4H), 7.50−7.43 (m, 9H). $^{13}C\{^{1}H\}$ NMR (100.6 MHz, $CDCl_3$) δ 143.9, 133.6, 129.7, 129.3, 129.1, 128.8, 125.5, 123.5 (t, $^{4}J_{CF}$ = 3 Hz). ^{11}B NMR (128.3 MHz, $CDCl_3$): δ –0.6 (t, $^{1}J_{BF}$ = 29 Hz). ^{19}F NMR (376.1 Hz, $CDCl_3$): δ –144.6 (q, $^{1}J_{FB}$ = 29 Hz). FT-IR (KBr): 3263 (m), 3035 (m), 2900 (m), 2889 (m), 1310 (m), 1290 (s), 1265 (s), 1218 (m), 1168 (m), 1113 (s) cm^{-1}. UV-vis (toluene): λ_{max} = 517 nm (ε = 23, 800 M^{-1} cm^{-1}). Mass Spec. (EI, +ve mode): exact mass calculated for $[C_{19}H_{15}N_4BF_2]^{+}$: 348.1358; exact mass found: 348.1374; difference: +4.7 ppm.

Formazanate BF_2 Complex 7b (Ar_1 = Ar_5 = Ph, R_3 = Np)

From 1.70 mmol of formazan **8b**: Yield = 0.31 g, 46%. Melting point = 127–129 °C. ^{1}H NMR (599.5 MHz, $CDCl_3$) δ 8.56 (s, 1H), 8.27–8.25 (m, 1H), 7.96–7.93 (m, 6H), 7.90–7.88 (m, 1H), 7.54–7.50 (m, 6H), 7.48–7.45 (m, 2H). $^{13}C\{^{1}H\}$ NMR (100.6 MHz, $CDCl_3$): δ 144.0, 134.0, 133.6, 131.1, 129.9, 129.3, 128.8, 128.7, 128.0, 126.8, 126.7, 125.1, 123.7 (t, $^{4}J_{CF}$ = 4 Hz), 123.1, 110.2. ^{11}B NMR (128.3 MHz, $CDCl_3$): δ –0.5 (t, $^{1}J_{BF}$ = 29 Hz). ^{19}F NMR (376.1 Hz, $CDCl_3$): δ –144.8 (q, $^{1}J_{FB}$ = 29 Hz). FT-IR (KBr): 3236 (m), 3055 (m), 2915 (m), 2860 (m), 1313 (s), 1279 (s), 1220 (m), 1172 (m), 1106 (m), 1105 (m) cm^{-1}. UV-vis (toluene): λ_{max} = 529 nm (ε = 20, 900 M^{-1} cm^{-1}). Mass Spec. (EI, +ve mode): exact mass calculated for $[C_{23}H_{17}N_4BF_2]^{+}$: 398.1514; exact mass found: 398.1513; difference: −0.3 ppm.

Formazanate BF_2 Complex 7c (Ar_1 = R_3 = Ph, Ar_5 = Np)

From 1.50 mmol of formazan **8c**: Yield = 0.44 g, 73%. Melting point = 106–108 °C. ^{1}H NMR (599.5 MHz, $CDCl_3$) δ 8.46 (s, 1H), 8.18–8.16 (m, 2H), 8.07–8.05 (m, 1H), 7.97–7.92 (m, 4H), 7.88–7.86 (m, 1H), 7.57–7.43 (m, 8H). $^{13}C\{^{1}H\}$ NMR (100.6 MHz, $CDCl_3$): δ 149.4, 144.1,

141.6, 133.8, 133.6, 133.2, 129.8, 129.5, 129.3, 129.3, 129.2, 128.9, 127.9, 127.8, 127.2, 125.7, 123.6 (t, $^4J_{CF}$ = 2 Hz), 123.4 (t, $^4J_{CF}$ = 4 Hz), 120.7. ^{11}B NMR (128.3 MHz, $CDCl_3$): δ –0.4 (t, $^1J_{BF}$ = 29 Hz). ^{19}F NMR (376.1 Hz, $CDCl_3$): δ –143.9 (q, $^1J_{FB}$ = 29 Hz). FT-IR (KBr): 3236 (m), 3059 (s), 2915 (m), 2845 (m), 1347 (m), 1341 (m), 1294 (s), 1266 (s), 1218 (m), 1174 (m) cm^{-1}. UV-vis (toluene): λ_{max} = 535 nm (ε = 26, 800 M^{-1} cm^{-1}). Mass Spec. (EI, +ve mode): exact mass calculated for $[C_{23}H_{17}N_4BF_2]^+$: 398.1514; exact mass found: 398.1512; difference: −0.6 ppm.

Formazanate BF_2 Complex 7d (Ar_1 = Ar_5 = Np, R_3 = Ph)

From 2.70 mmol of formazan **8d**: Yield = 0.95 g, 78%. Melting point = 140–142 °C. ^{1}H NMR (599.5 MHz, $CDCl_3$) δ 8.49 (s, 2H), 8.21 (d, $^3J_{HH}$ = 7 Hz, 2H), 8.10–8.08 (m, 2H), 7.97–7.93 (m, 4H), 7.89–7.86 (m, 2H), 7.57–7.48 (m, 7H). ^{13}C{^{1}H} NMR (100.6 MHz, $CDCl_3$): δ 141.6, 133.9, 133.5, 133.1, 129.4, 129.3, 129.3, 128.9, 127.9, 127.7, 127.1, 125.7, 123.3 (t, $^4J_{CF}$ = 4 Hz), 120.6, 119.1. ^{11}B NMR (128.3 MHz, $CDCl_3$): δ –0.2 (t, $^1J_{BF}$ = 29 Hz). ^{19}F NMR (376.1 Hz, $CDCl_3$): δ –143.3 (q, $^1J_{FB}$ = 29 Hz). FT-IR (KBr): 3276 (m), 3050 (s), 2915 (m), 2846 (m), 1626 (m), 1592 (m), 1507 (s), 1344 (s), 1298 (s), 1265 (m) cm^{-1}. UV-vis (toluene): λ_{max} = 556 nm (ε = 25, 200 M^{-1} cm^{-1}). Mass Spec. (ESI, +ve mode): exact mass calculated for $[C_{27}H_{19}N_4BF_2Na]^+$: 471.1568; exact mass found: 471.1569; difference: +0.1 ppm.

Formazanate BF_2 Complex 7f (Ar_1 = Ar_5 = Np, R_3 = CN)

From 2.30 mmol of formazan **8f**: Yield = 0.74 g, 81%. Melting point = 118–120 °C. ^{1}H NMR (599.5 MHz, $CDCl_3$) δ 8.51 (s, 2H), 8.03–8.01 (m, 2H), 7.98–7.93 (m, 4H), 7.89–7.87 (m, 2H), 7.62–7.56 (m, 4H). ^{13}C{^{1}H} NMR (100.6 MHz, $CDCl_3$): δ 141.0, 134.4, 133.1, 130.1, 129.9, 129.0, 128.2, 127.8, 126.4, 124.2, 119.5 (t, $^4J_{CF}$ = 3 Hz), 114.5. ^{11}B NMR (128.3 MHz, $CDCl_3$): δ –0.4 (t, $^1J_{BF}$ = 31 Hz). ^{19}F NMR (376.1 Hz, $CDCl_3$): δ –132.7 (q, $^1J_{FB}$ = 31 Hz). FT-IR (KBr):

3235 (m), 3035 (m), 2895 (m), 2240 (s), 1350 (s), 1146 (m), 1124 (m), 1028 (m) cm^{-1}. UV-vis (toluene): λ_{max} = 581 nm (ε = 25, 700 M^{-1} cm^{-1}). Mass Spec. (EI, +ve mode): exact mass calculated for $[C_{22}H_{14}N_5BF_2]^+$: 397.1310; exact mass found: 397.1311; difference: +0.2 ppm.

Formazanate BF_2 Complex 7g (Ar_1 = Ar_5 = Ph, R_3 = NO_2)

From 2.90 mmol of formazan **8g**: Yield = 0.27 g, 29%. Melting point = 108–110 °C. ^{1}H NMR (399.8 MHz, $CDCl_3$) δ 8.01–7.99 (m, 4H), 7.56–7.52 (m, 6H). $^{13}C\{^1H\}$ NMR (100.6 MHz, $CDCl_3$): δ 143.4, 132.2, 129.9, 123.7 (t, $^4J_{CF}$ = 2 Hz). ^{11}B NMR (128.3 MHz, $CDCl_3$): δ –0.7 (t, $^1J_{BF}$ = 30 Hz). ^{19}F NMR (376.1 Hz, $CDCl_3$): δ –135.4 (q, $^1J_{FB}$ = 29 Hz). FT-IR (KBr): 3257 (m), 3062 (m), 2915 (m), 2912 (m), 2844 (m), 1557 (s), 1417 (s), 1333 (s), 1327 (s), 1271 (m), 1175 (m), 1151 (m) cm^{-1}. UV-vis (toluene): λ_{max} = 505 nm (ε = 26, 000 M^{-1} cm^{-1}). Mass Spec. (EI, +ve mode): exact mass calculated for $[C_{13}H_{10}N_5O_2BF_2]^+$: 317.0896; exact mass found: 317.0901; difference: +1.7 ppm.

Formazanate BF_2 Complex 7h (Ar_1 = Ar_5 = Np, R_3 = NO_2)

From 0.54 mmol of formazan **8h**: Yield = 0.22 g, 99%. Melting point = 199–201 °C. ^{1}H NMR (599.5 MHz, $CDCl_3$) δ 8.61 (s, 2H), 8.14 (d, $^3J_{HH}$ = 9 Hz, 2H), 8.01–7.97 (m, 4H), 7.90 (d, $^3J_{HH}$ = 8 Hz, 2H), 7.65–7.58 (m, 4H). $^{13}C\{^1H\}$ NMR (100.6 MHz, $CDCl_3$): δ 141.1, 134.6, 133.1, 130.4, 130.3, 129.9, 129.2, 128.2, 127.8, 124.6 (t, $^4J_{CF}$ = 4 Hz), 119.5. ^{11}B NMR (128.3 MHz, $CDCl_3$): δ –0.3 (t, $^1J_{BF}$ = 29 Hz). ^{19}F NMR (376.1 Hz, $CDCl_3$): δ –134.3 (q, $^1J_{FB}$ = 29 Hz). FT-IR (KBr): 3270 (s), 3036 (m), 2888 (m), 1554 (s), 1538 (m), 1425 (m), 1377 (m), 1317 (s), 1269 (w) cm^{-1}. UV-vis (toluene): λ_{max} = 583 nm (ε = 24, 100 M^{-1} cm^{-1}). Mass Spec. (EI, +ve mode): exact mass calculated for $[C_{21}H_{14}N_5O_2BF_2]^+$: 417.1209; exact mass found: 417.1208; difference: −0.24 ppm.

Acknowledgements

This work was supported by the Natural Sciences and Engineering Research Council (NSERC) of Canada Discovery Grants (J. B. G. and V. N. S.) and Canada Graduate Scholarships program (S. M. B.) and by The University of Western Ontario. We thank Prof. Elizabeth R. Gillies for access to instruments in her lab.

Associated Content

Supporting Information: ^{1}H and ^{13}C NMR spectra, UV-vis absorption and emission spectra, cyclic voltammograms, computational details and a .cif file for **7g**. This material is available free of charge via the Internet at http://pubs.acs.org/.

Author Information

Corresponding Author

*Email: joe.gilroy@uwo.ca. Phone: +1-519-661-2111 ext. 81561.

Notes

The authors declare no competing financial interest.

References

(1) Murov, S. L. *Handbook of Photochemistry*; Marcel Dekker, Inc.: New York, 1973.

(2) Roncali, J.; Leriche, P.; Blanchard, P. *Adv. Mater.* **2014**, *26*, 3821−3838.

(3) Frath, D.; Massue, J.; Ulrich, G.; Ziessel, R. *Angew. Chem. Int. Ed.* **2014**, *53*, 2290−2310.

(4) Wu, W.; Liu, Y.; Zhu, D. *Chem. Soc. Rev.* **2010**, *39*, 1489−1502.

(5) Mei, J.; Hong, Y.; Lam, J. W. Y.; Qin, A.; Tang, Y.; Tang, B. Z. *Adv. Mater.* **2014**, *26*, 5429−5479.

(6) For example: (a) Qian, B.; Baek, S. W.; Smith III, M. R. *Polyhedron* **1999**, *18*, 2405−2414; (b) Norman, D. W.; Edwards, J. P.; Vogels, C. M.; Decken, A.; Westcott, S. A. *Can. J. Chem.*

2002, *80*, 31−40; (c) Liddle, B. J.; Silva, R. M.; Morin, T. J.; Macedo, F. P.; Shukla, R.; Lindeman, S. V.; Gardinier, J. R. *J. Org. Chem.* **2007**, *72*, 5637−5646; (d) Kubota, Y.; Tsuzuki, T.; Funabiki, K.; Ebihara, M.; Matsui, M. *Org. Lett.* **2010**, *12*, 4010−4013; (e) Oakley, S. R.; Nawn, G.; Waldie, K. M.; MacInnis, T. D.; Patrick, B. O.; Hicks, R. G. *Chem. Commun.* **2010**, *46*, 6753−6755; (f) Cheng, F.; Jäkle, F. *Chem. Commun.* **2010**, *46*, 3717−3719; (g) Liu, T.; Chien, A. D.; Lu, J.; Zhang, G.; Fraser, C. L. *J. Mater. Chem.* **2011**, *21*, 8401−8408; (h) Bonnier, C.; Machin, D. D.; Abdi, O.; Koivisto, B. D. *Org. Biomol. Chem.* **2013**, *11*, 3756−3760; (i) Kubota, Y.; Ozaki, Y.; Funabiki, K.; Matsui, M. *J. Org. Chem.* **2013**, *78*, 7058−7067; (j) Albrett, A. M.; Thomas, K. E.; Maslek, S.; Młodzianowska, A.; Conradie, J.; Beavers, C. M.; Ghosh, A.; Brothers, P. J. *Inorg. Chem.* **2014**, *53*, 5486−5493; (k) Barbon, S. M.; Staroverov, V. N.; Boyle, P. D.; Gilroy, J. B. *Dalton Trans.* **2014**, *43*, 240−250; (l) Liao, C.-W.; Rajeswara, R. M.; Sun, S.-S. *Chem. Commun.* **2015**, *51*, 2656−2659; (m) Kubota, Y.; Kasatani, K.; Takai, H.; Funabiki, K.; Matsui, M. *Dalton Trans.* **2015**, *44*, 3326−3341.

(7) Reviews: (a) Loudet, A.; Burgess, K. *Chem. Rev.* **2007**, *107*, 4891−4932; (b) Ulrich, G.; Ziessel, R.; Harriman, A. *Angew. Chem. Int. Ed.* **2008**, *47*, 1184−1201; (c) Boens, N.; Leen, V.; Dehaen, W. *Chem. Soc. Rev.* **2012**, *41*, 1130−1172.

(8) For example: (a) Chen, J.; Burghart, A.; Derecskei-Kovacs, A.; Burgess, K. *J. Org. Chem.* **2000**, *65*, 2900−2906; (b) Ueno, Y.; Jose, J.; Loudet, A.; Pérez-Bolívar, C.; Anzenbacher, P.; Burgess, K. *J. Am. Chem. Soc.* **2011**, *133*, 51−55; (c) Niu, S.; Ulrich, G.; Retailleau, P.; Ziessel, R. *Tetrahedron Lett.* **2011**, *52*, 4848−4853; (d) Nepomnyashchii, A. B.; Bröring, M.; Ahrens, J.; Bard, A. J. *J. Am. Chem. Soc.* **2011**, *133*, 8633−8645; (e) Lu, J.-s.; Ko, S.-B.; Walters, N. R.; Wang, S. *Org. Lett.* **2012**, *14*, 5660−5663; (f) Zhang, X.; Yu, H.; Xiao, Y. *J. Org. Chem.* **2012**, *77*, 669−673; (g) Jameson, L. P.; Dzyuba, S. V. *Bioorg. Med. Chem. Lett.* **2013**, *23*, 1732−1735;

(h) Manjare, S. T.; Kim, J.; Lee, Y.; Churchill, D. G. *Org. Lett.* **2014**, *16*, 520−523; (i) Frenette, M.; Hatamimoslehabadi, M.; Bellinger-Buckley, S.; Laoui, S.; La, J.; Bag, S.; Mallidi, S.; Hasan, T.; Bouma, B.; Yelleswarapu, C.; Rochford, J. *J. Am. Chem. Soc.* **2014**, *136*, 15853−15856; (j) Shie, J.-J.; Liu, Y.-C.; Lee, Y.-M.; Lim, C.; Fang, J.-M.; Wong, C.-H. *J. Am. Chem. Soc.* **2014**, *136*, 9953−9961; (k) Bandi, V.; Das, S. K.; Awuah, S. G.; You, Y.; D'Souza, F. *J. Am. Chem. Soc.* **2014**, *136*, 7571−7574; (l) Bruhn, T.; Pescitelli, G.; Jurinovich, S.; Schaumlöffel, A.; Witterauf, F.; Ahrens, J.; Bröring, M.; Bringmann, G. *Angew. Chem. Int. Ed.* **2014**, *53*, 14592−14595; (m) Raut, S.; Kimball, J.; Fudala, R.; Doan, H.; Maliwal, B.; Sabnis, N.; Lacko, A.; Gryczynski, I.; Dzyuba, S. V.; Gryczynski, Z. *Phys. Chem. Chem. Phys.* **2014**, *16*, 27037−27042; (n) Lakshmi, V.; Ravikanth, M. *RSC Adv.* **2014**, *4*, 44327−44336.

(9) Kollmannsberger, M.; Rurack, K.; Resch-Genger, U.; Daub, J. *J. Phys. Chem. A* **1998**, *102*, 10211−10220.

(10) Shen, Z.; Röhr, H.; Rurack, K.; Uno, H.; Spieles, M.; Schulz, B.; Reck, G.; Ono, N. *Chem. Eur. J.* **2004**, *10*, 4853−4871.

(11) Quan, L.; Chen, Y.; Lv, X.-J.; Fu, W.-F. *Chem. Eur. J.* **2012**, *18*, 14599−14604.

(12) Araneda, J. F.; Piers, W. E.; Heyne, B.; Parvez, M.; McDonald, R. *Angew. Chem. Int. Ed.* **2011**, *50*, 12214−12217.

(13) Reviews: (a) Nineham, A. W. *Chem. Rev.* **1955**, *55*, 355-483; (b) Sigeiken, G. I.; Lipunova, G. N.; Pervova, I. G. *Russ. Chem. Rev.* **2006**, *75*, 885−900.

(14) (a) Chang, M.-C.; Otten, E. *Chem. Commun.* **2014**, *50*, 7431−7433; (b) Barbon, S. M.; Reinkeluers, P. A.; Price, J. T.; Staroverov, V. N.; Gilroy, J. B. *Chem. Eur. J.* **2014**, *20*, 11340−11344; (c) Barbon, S. M.; Price, J. T.; Reinkeluers, P. A.; Gilroy, J. B. *Inorg. Chem.* **2014**, *53*, 10585−10593.

(15) Hesari, M.; Barbon, S. M.; Staroverov, V. N.; Ding, Z.; Gilroy, J. B. *Chem. Commun.* **2015**, *51*, 3766−3769.

(16) (a) Ibrahim, Y. A.; Elwahy, A. H. M.; Abbas, A. A. *Tetrahedron* **1994**, *50*, 11489−11498; (b) Katritzky, A. A.; Belyakov, S. A.; Cheng, D.; Durst, H. D. *Synthesis* **1995**, *1995*, 577−581; (c) Gilroy, J. B.; McKinnon, S. D. J.; Koivisto, B. D.; Hicks, R. G. *Org. Lett.* **2007**, *9*, 4837−4840; (d) Gilroy, J. B.; Otieno, P. O.; Ferguson, M. J.; McDonald, R.; Hicks, R. G. *Inorg. Chem.* **2008**, *47*, 1279−1286.

(17) Gilroy, J. B.; Ferguson, M. J.; McDonald, R.; Patrick, B. O.; Hicks, R. G. *Chem. Commun.* **2007**, 126−128.

(18) For example: (a) Gilroy, J. B.; Ferguson, M. J.; McDonald, R.; Hicks, R. G. *Inorg. Chim. Acta* **2008**, *361*, 3388−3393; (b) Gilroy, J. B.; Patrick, B. O.; McDonald, R.; Hicks, R. G. *Inorg. Chem.* **2008**, *47*, 1287−1294; (c) Hong, S.; Gupta, A. K.; Tolman, W. B. *Inorg. Chem.* **2009**, *48*, 6323−6325; (d) Hong, S.; Hill, L. M. R.; Gupta, A. K.; Naab, B. D.; Gilroy, J. B.; Hicks, R. G.; Cramer, C. J.; Tolman, W. B. *Inorg. Chem.* **2009**, *48*, 4514−4523; (e) Lipunova, G. N.; Rezinskikh, Z. G.; Maslakova, T. I.; Slepukhin, P. A.; Pervova, I. G.; Lipunov, I. N.; Sigeikin, G. I. *Russ. J. Coord. Chem.* **2009**, *35*, 215−221; (f) Zaidman, A. V.; Pervova, I. G.; Vilms, A. I.; Belov, G. P.; Kayumov, R. R.; Slepukhin, P. A.; Lipunov, I. N. *Inorg. Chim. Acta* **2011**, *367*, 29−34; (g) Chang, M.-C.; Dann, T.; Day, D. P.; Lutz, M.; Wildgoose, G. G.; Otten, E. *Angew. Chem. Intl. Ed.* **2014**, *53*, 4118−4122; (h) Travieso-Puente, R.; Chang, M.-C.; Otten, E. *Dalton Trans.* **2014**, *43*, 18035−18041; (i) Chang, M.-C.; Roewen, P.; Travieso-Puente, R.; Lutz, M.; Otten, E. *Inorg. Chem.* **2015**, *54*, 379−388.

(19) Fery-Forgues, S.; Lavabre, D. *J. Chem. Educ.* **1999**, *76*, 1260−1264.

(20) Suzuki, K.; Kobayashi, A.; Kaneko, S.; Takehira, K.; Yoshihara, T.; Ishida, H.; Shiina, Y.; Oishi, S.; Tobita, S. *Phys. Chem. Chem. Phys.* **2009**, *11*, 9850−9860.

(21) *CRC Handbook of Chemistry and Physics*; CRC Press: Boca Raton, Fla, 2012.

(22) Gaussian 09, Revision **B.01**, Frisch, M. J.; Trucks, G. W.; Schlegel, H. B.; Scuseria, G. E.; Robb, M. A.; Cheeseman, J. R.; Scalmani, G.; Barone, V.; Mennucci, B.; Petersson, G. A.; Nakatsuji, H.; Caricato, M.; Li, X.; Hratchian, H. P.; Izmaylov, A. F.; Bloino, J.; Zheng, G.; Sonnenberg, J. L.; Hada, M.; Ehara, M.; Toyota, K.; Fukuda, R.; Hasegawa, J.; Ishida, M.; Nakajima, T.; Honda, Y.; Kitao, O.; Nakai, H.; Vreven, T.; Montgomery, Jr., J. A.; Peralta, J. E.; Ogliaro, F.; Bearpark, M.; Heyd, J. J.; Brothers, E.; Kudin, K. N.; Staroverov, V. N.; Kobayashi, R.; Normand, J.; Raghavachari, K.; Rendell, A.; Burant, J. C.; Iyengar, S. S.; Tomasi, J.; Cossi, M.; Rega, N.; Millam, J. M.; Klene, M.; Knox, J. E.; Cross, J. B.; Bakken, V.; Adamo, C.; Jaramillo, J.; Gomperts, R.; Stratmann, R. E.; Yazyev, O.; Austin, A. J.; Cammi, R.; Pomelli, C.; Ochterski, J. W.; Martin, R. L.; Morokuma, K.; Zakrzewski, V. G.; Voth, G. A.; Salvador, P.; Dannenberg, J. J.; Dapprich, S.; Daniels, A. D.; Farkas, Ö.; Foresman, J. B.; Ortiz, J. V.; Cioslowski, J.; Fox, D. J. Gaussian, Inc., Wallingford CT, 2009.

(23) Zhao, Y.; Truhlar, D. G. *Theor. Chem. Acc.* **2008**, *120*, 215-241.

(24) Bruker-AXS, SAINT version 2013.8, **2013**, Bruker-AXS, Madison, WI 53711, USA.

(25) Bruker-AXS, SADABS version 2012.1, **2012**, Bruker-AXS, Madison, WI 53711, USA.

(26) Sheldrick, G. M. *Acta Cryst.* **2015**, *A71*, 3−8.

(27) Sheldrick, G. M. *Acta Cryst.* **2008**, *A64*, 112−122.

Supporting Information

The Effect of Extended π-Conjugation on the Spectroscopic and Electrochemical Properties of Boron Difluoride Formazanate Complexes

*Stephanie M. Barbon, Viktor N. Staroverov and Joe B. Gilroy**

Department of Chemistry and the Centre for Advanced Materials and Biomaterials Research (CAMBR), The University of Western Ontario, 1151 Richmond St. N., London, Ontario, Canada, N6A 5B7. Tel: +1-519-661-2111 ext. 81561; E-mail: joe.gilroy@uwo.ca

Table of Contents

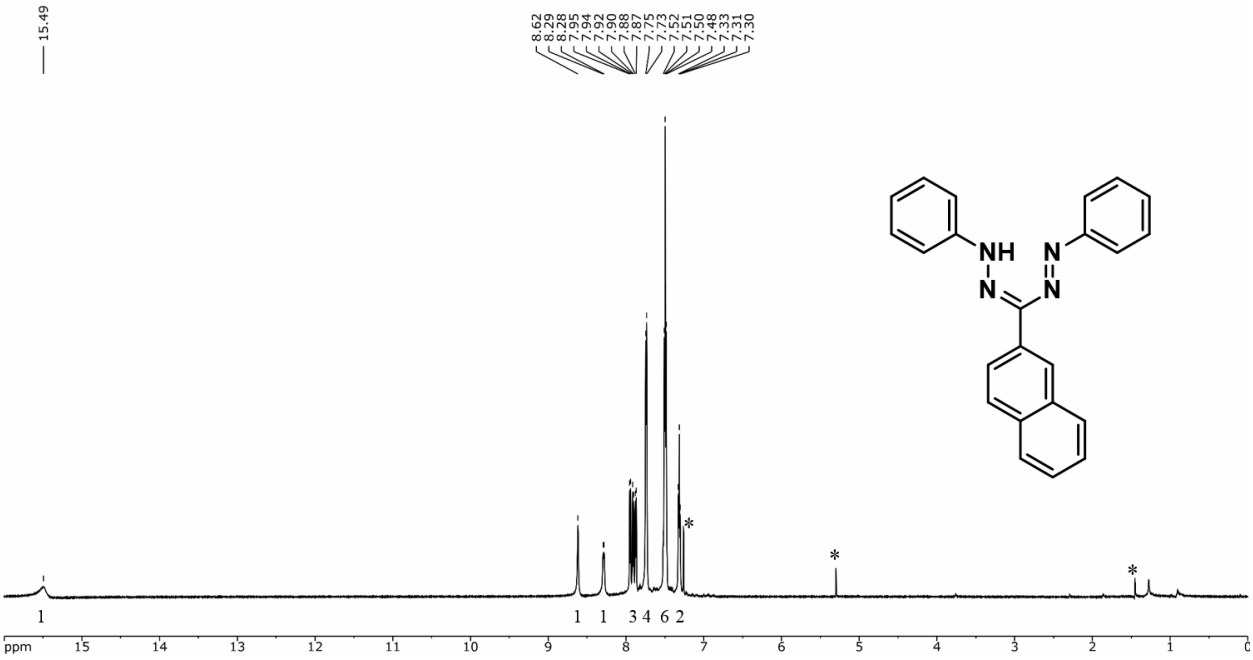

Figure S1. ^{1}H NMR spectrum of **8b** in $CDCl_3$. The asterisks denote residual solvent signals.

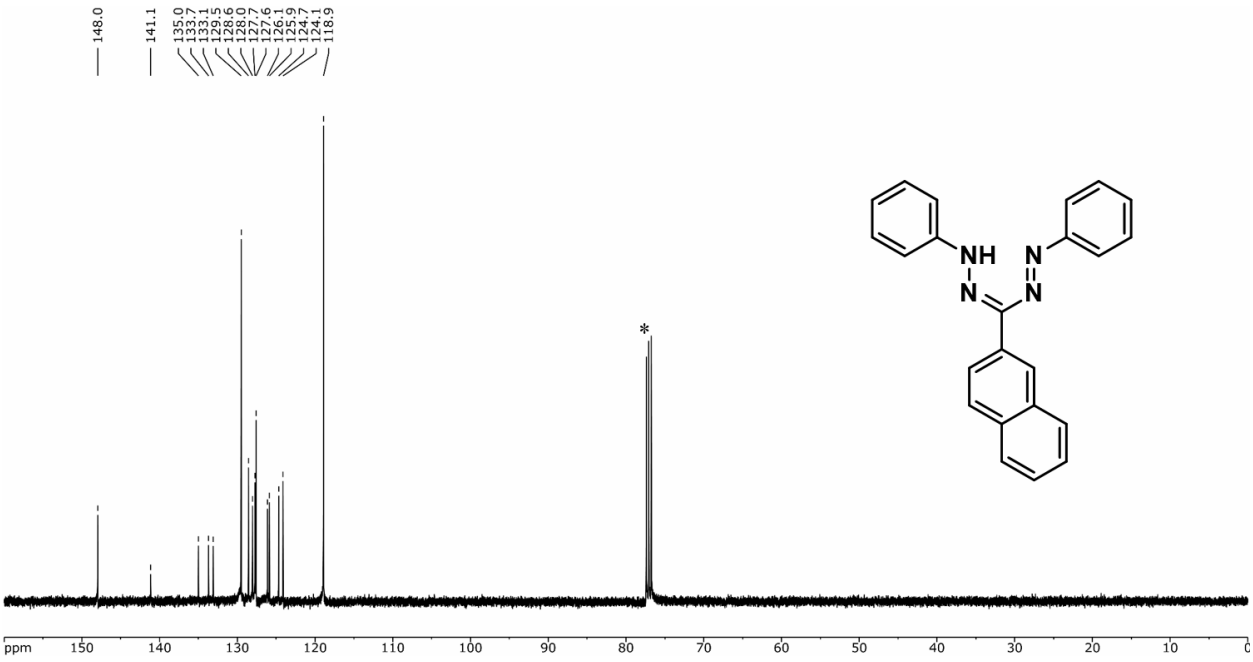

Figure S2. $^{13}C\{^{1}H\}$ NMR spectrum of **8b** in $CDCl_3$. The asterisk denotes $CDCl_3$ solvent signal.

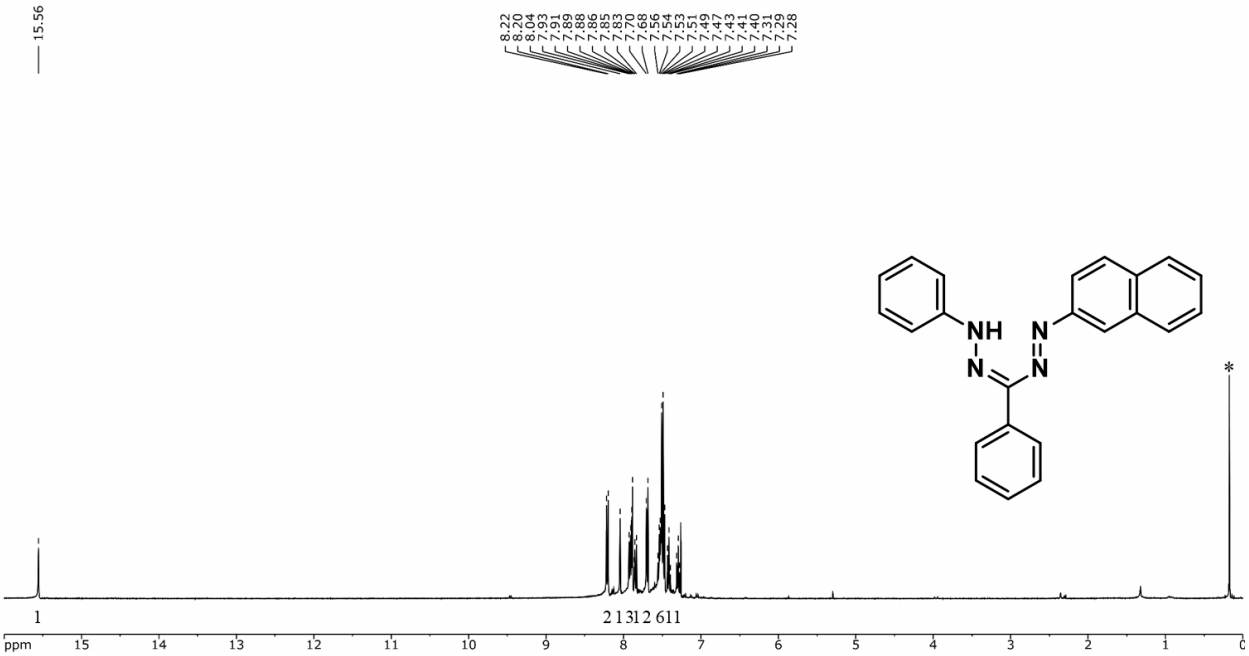

Figure S3. ^{1}H NMR spectrum of **8c** in $CDCl_3$. The asterisks denote residual grease signal.

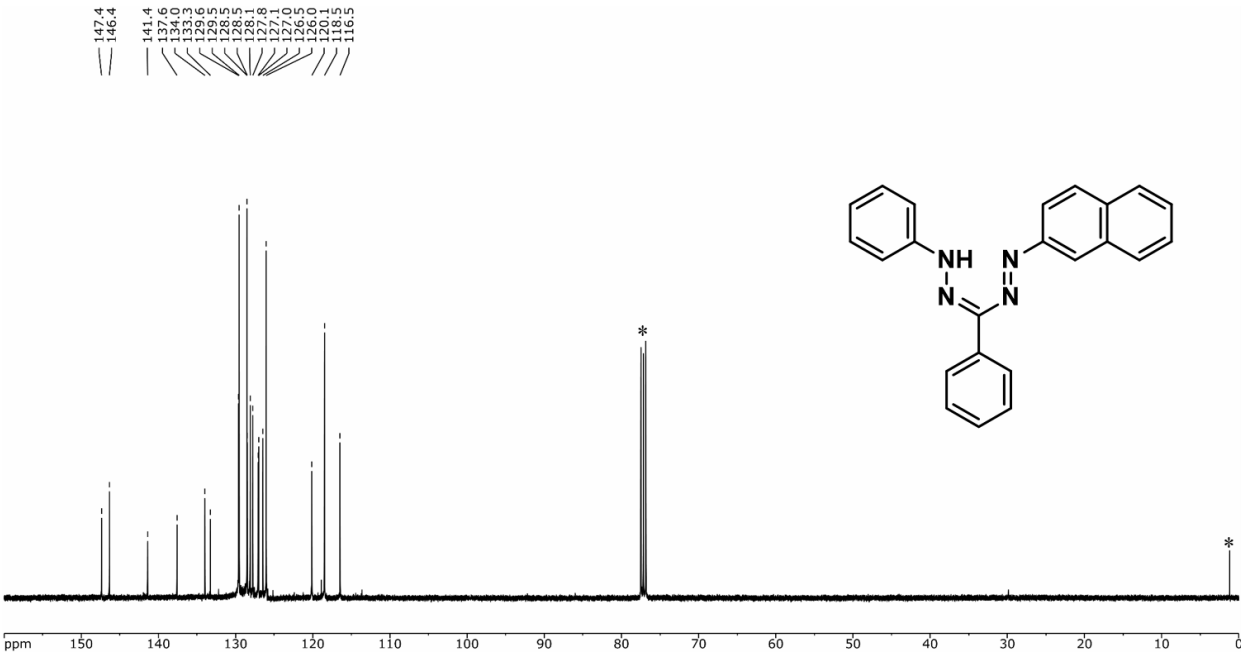

Figure S4. $^{13}C\{^{1}H\}$ NMR spectrum of **8c** in $CDCl_3$. The asterisks denote $CDCl_3$ solvent/grease signal.

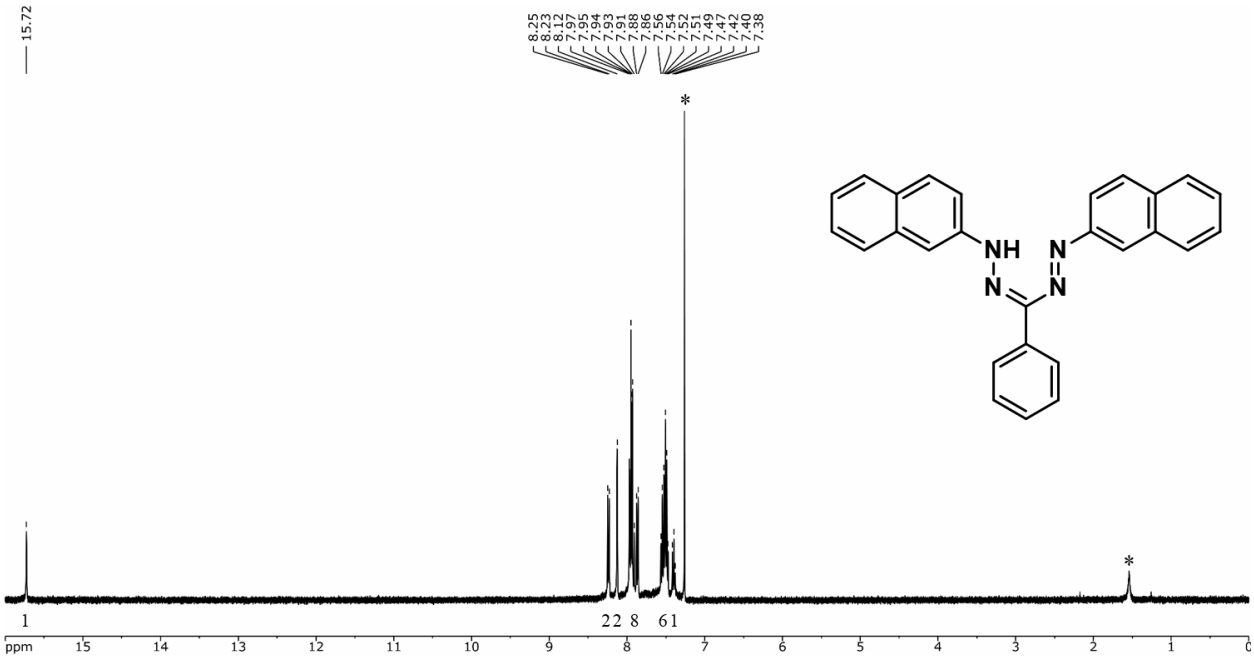

Figure S5. ^{1}H NMR spectrum of **8d** in $CDCl_3$. The asterisks denote residual solvent signals.

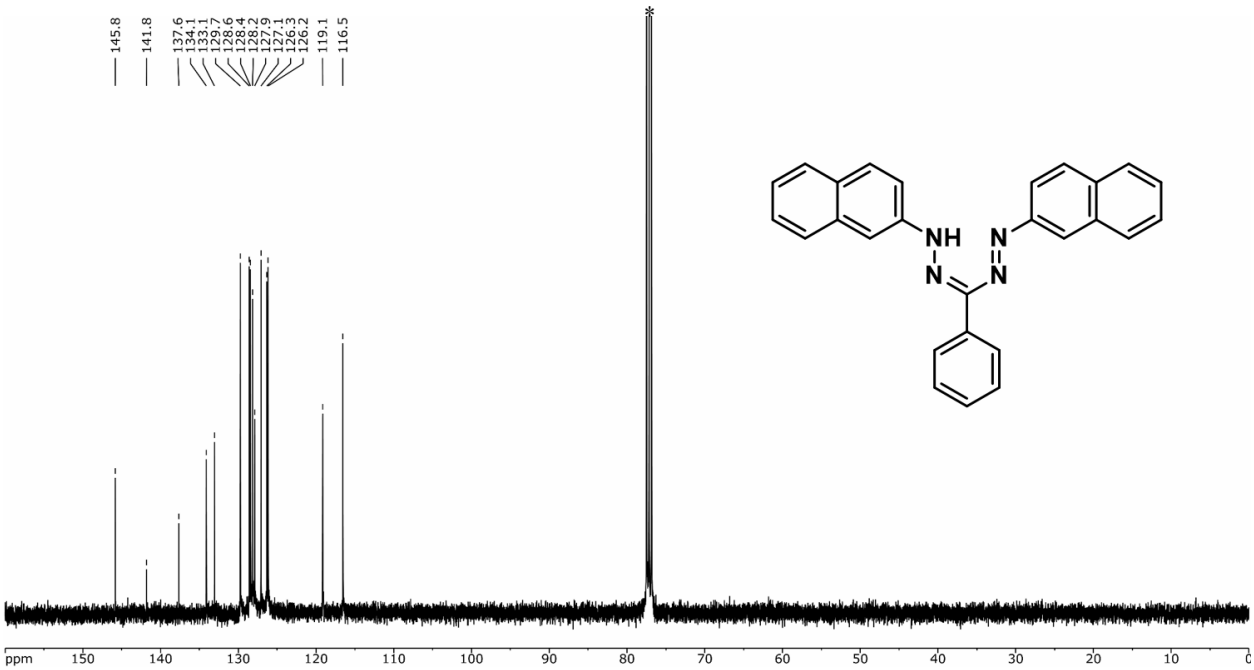

Figure S6. $^{13}C\{^{1}H\}$ NMR spectrum of **8d** in $CDCl_3$. The asterisk denotes residual $CDCl_3$ signal.

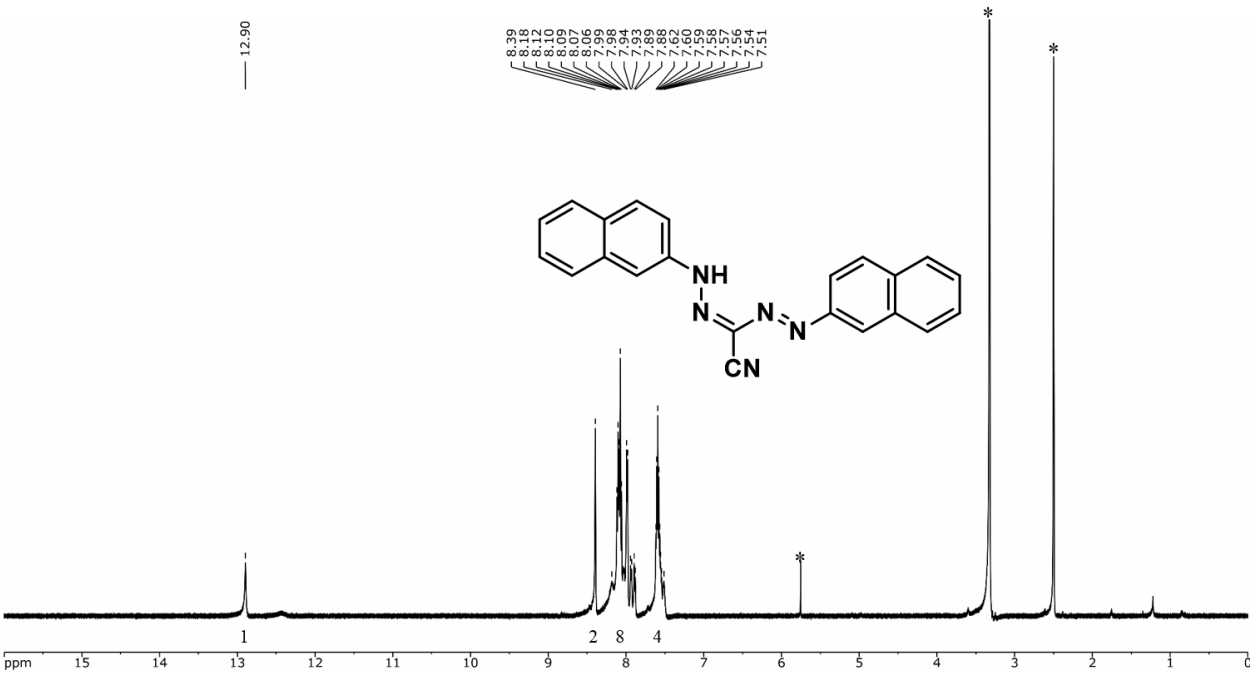

Figure S7. ^{1}H NMR spectrum of **8f** in DMSO-d_6. The asterisks denote residual solvent signals.

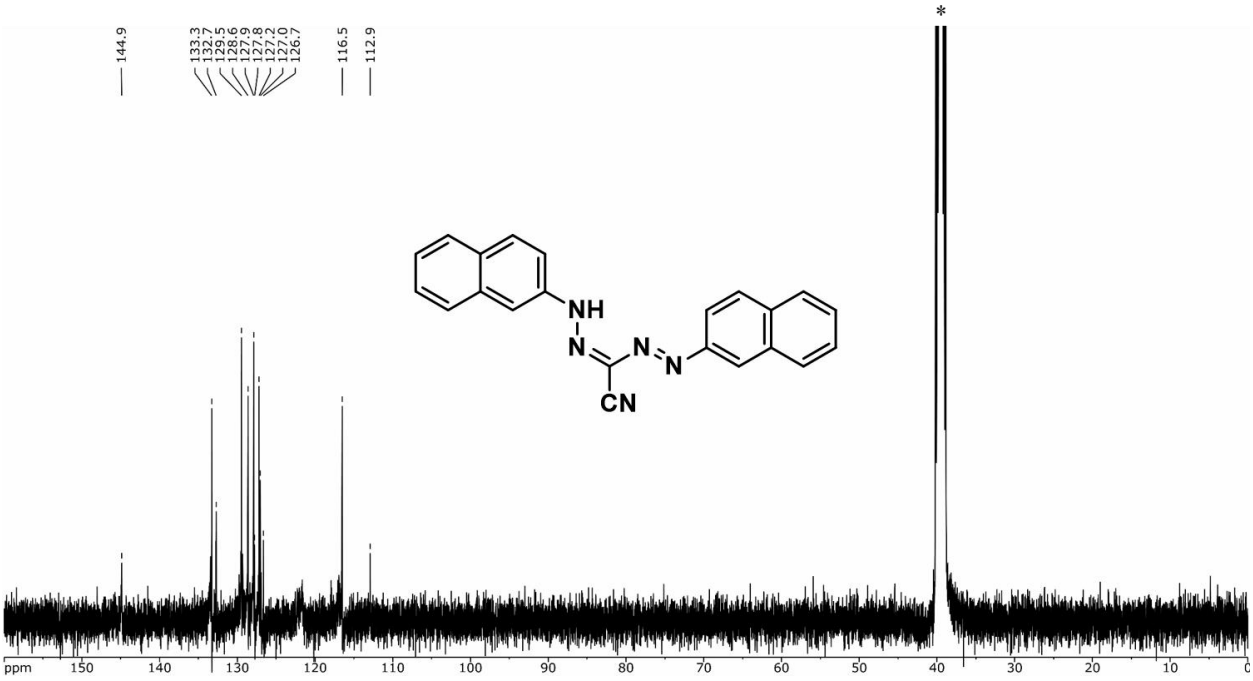

Figure S8. ^{13}C{^{1}H} NMR spectrum of **8f** in DMSO-d_6. The asterisk denotes residual DMSO-d_6 signal. This spectrum was measured for 10,000 scans on a 400 MHz spectrometer. The poor signal-to-noise ratio relates to the poor solubility of **8f**.

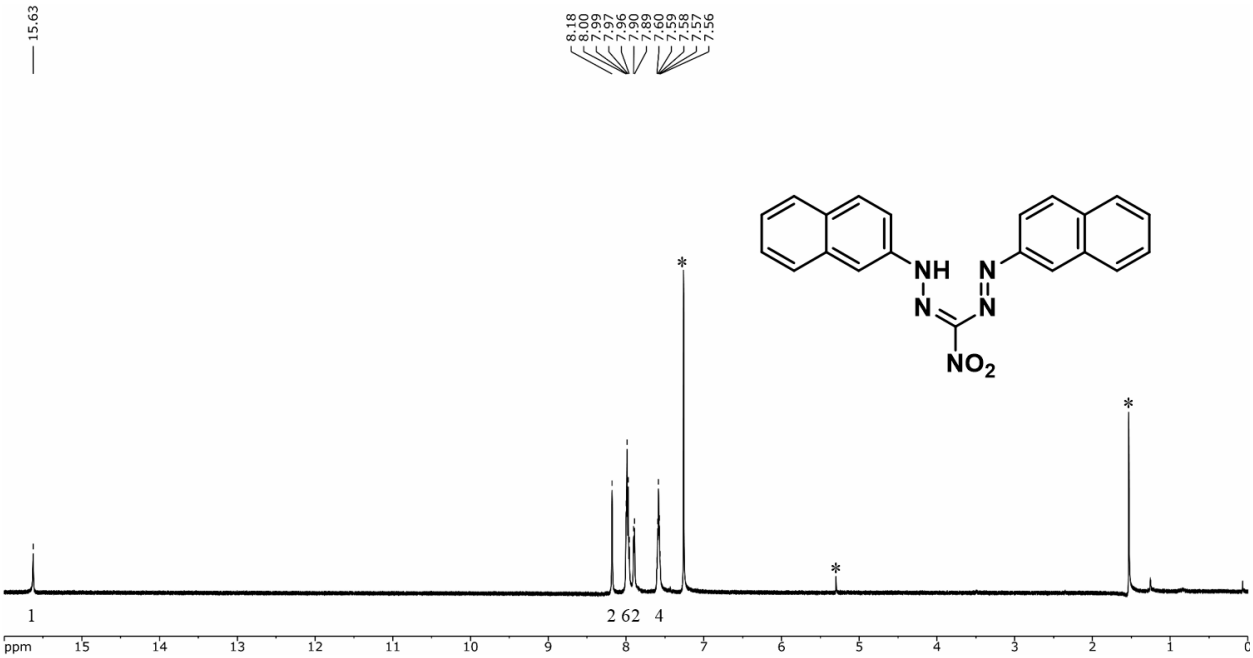

Figure S9. ^{1}H NMR spectrum of **8h** in $CDCl_3$. The asterisks denote residual solvent signals.

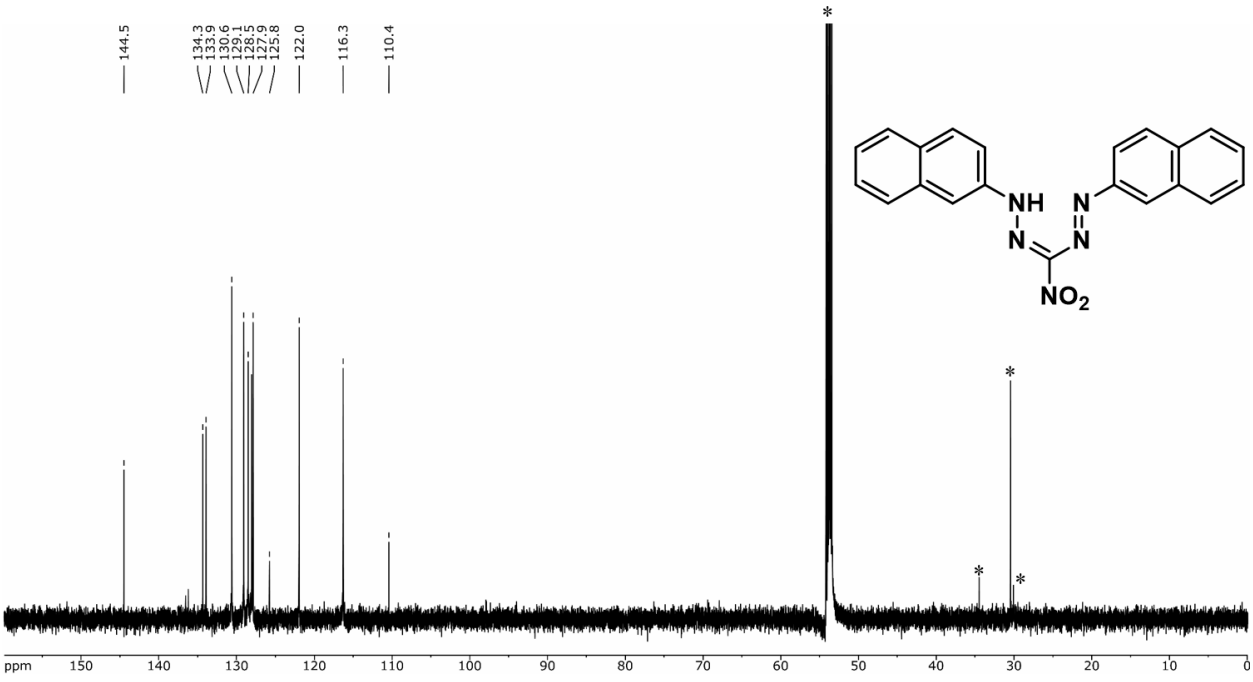

Figure S10. $^{13}C\{^{1}H\}$ NMR spectrum of **8h** in CD_2Cl_2. The asterisks denote CD_2Cl_2 solvent and solvent impurity signals.

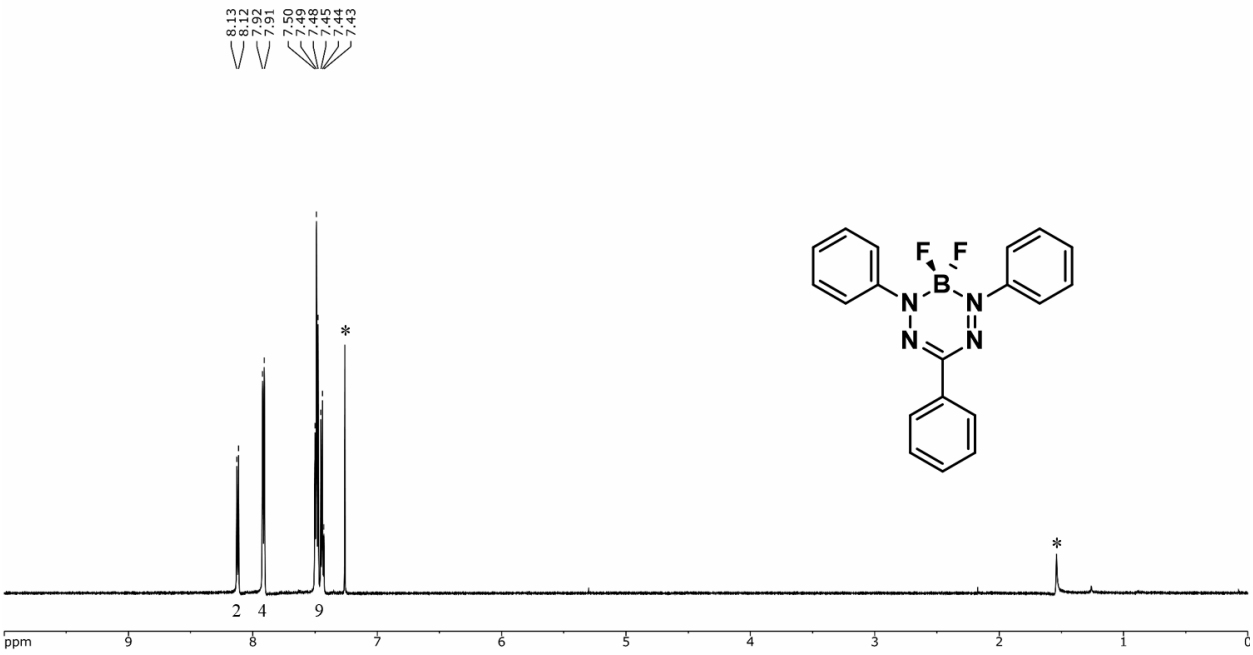

Figure S11. ^{1}H NMR spectrum of **7a** in $CDCl_3$. The asterisk denotes residual solvent signals.

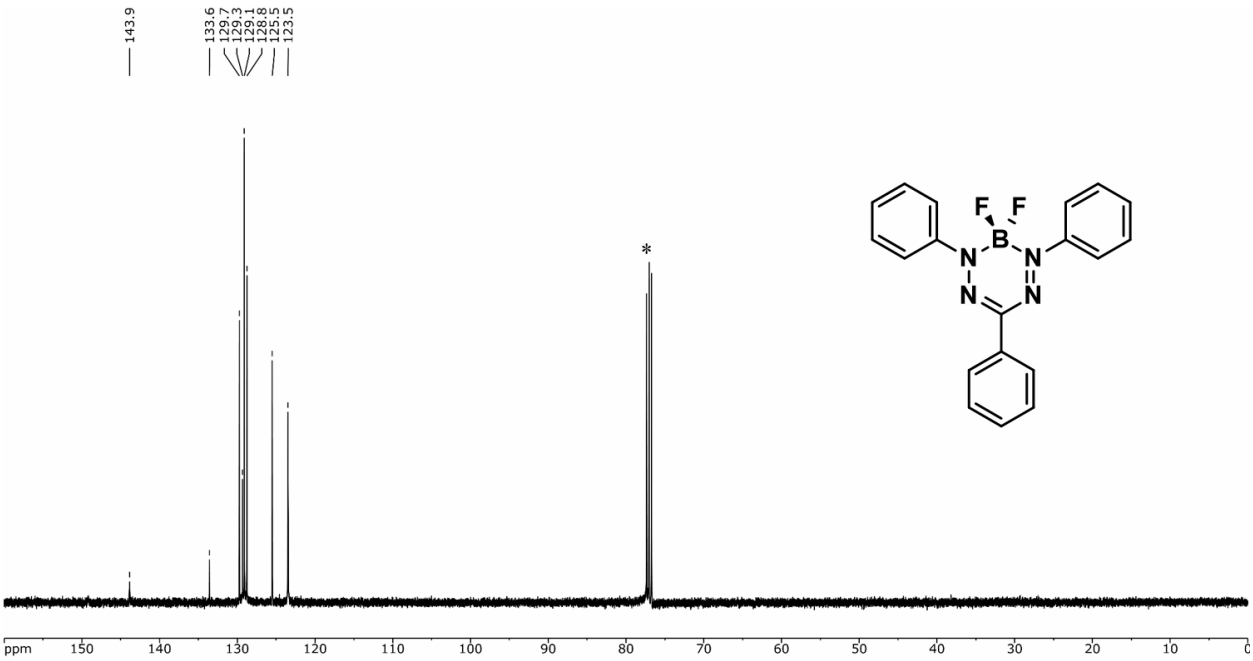

Figure S12. $^{13}C\{^{1}H\}$ NMR spectrum of **7a** in $CDCl_3$. The asterisk denotes $CDCl_3$ solvent signal.

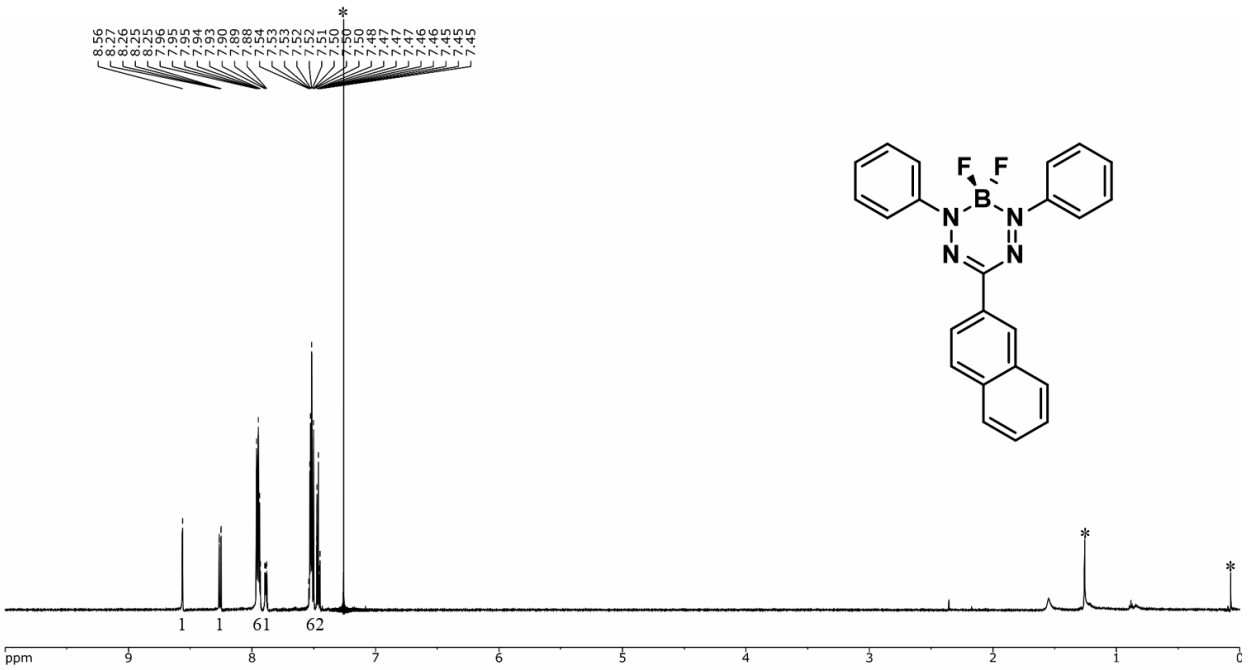

Figure S13. ^{1}H NMR spectrum of **7b** in $CDCl_3$. The asterisks denote residual solvent/grease signals.

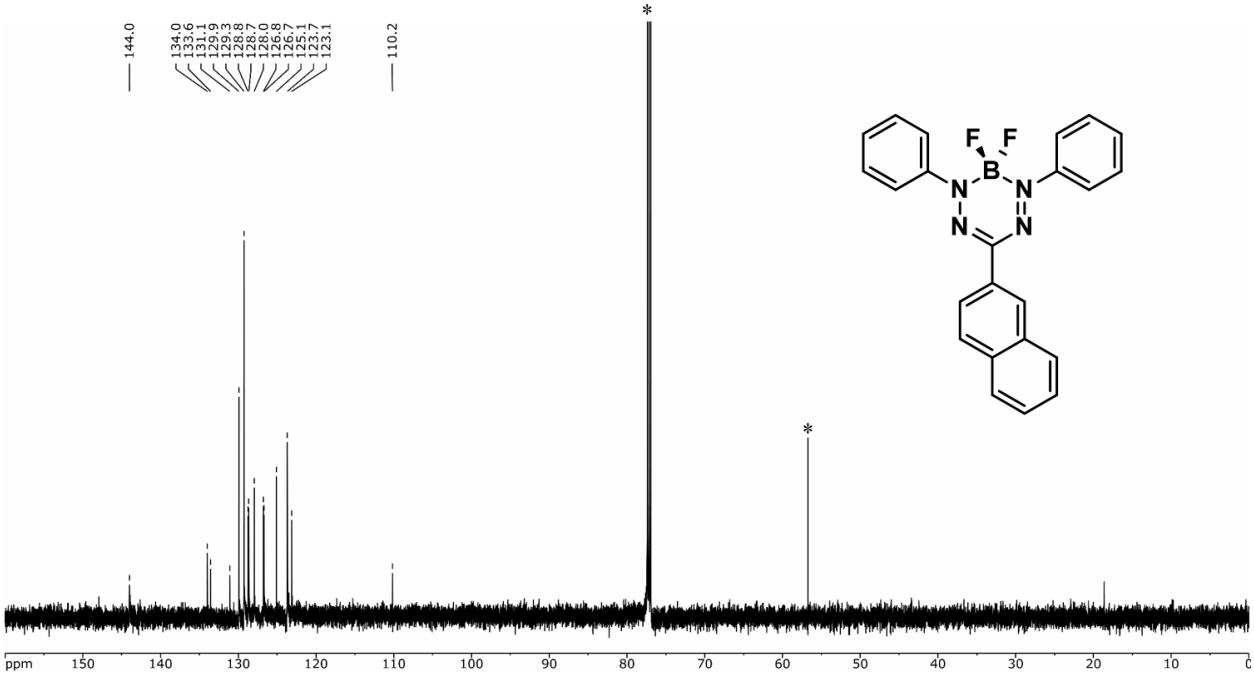

Figure S14. $^{13}C\{^{1}H\}$ NMR spectrum of **7b** in $CDCl_3$. The asterisk denotes $CDCl_3$ solvent signal.

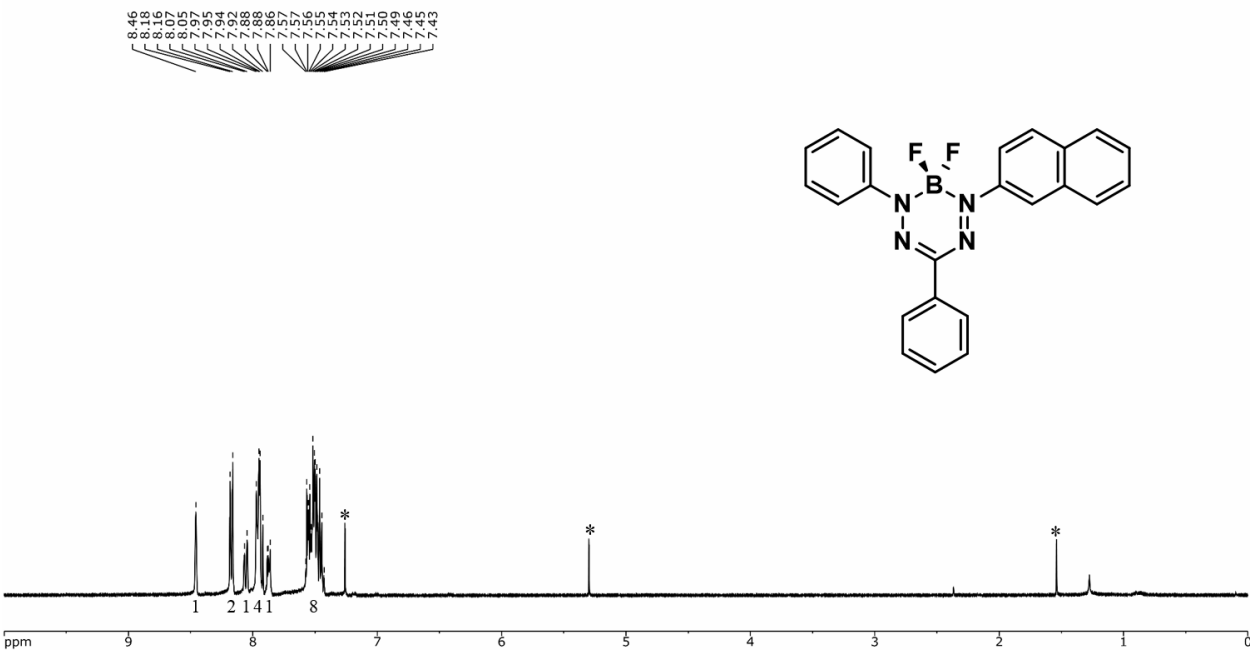

Figure S15. ^{1}H NMR spectrum of **7c** in $CDCl_3$. The asterisks denote residual solvent signals.

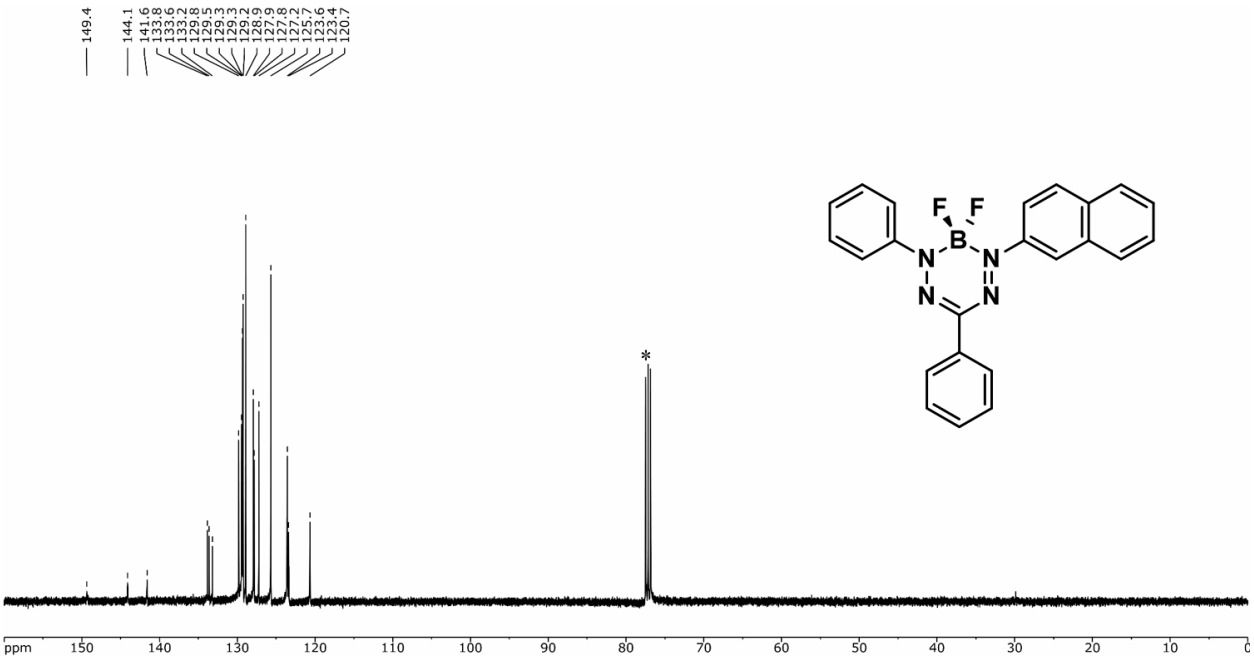

Figure S16. $^{13}C\{^{1}H\}$ NMR spectrum of **7c** in $CDCl_3$. The asterisk denotes $CDCl_3$ solvent signal.

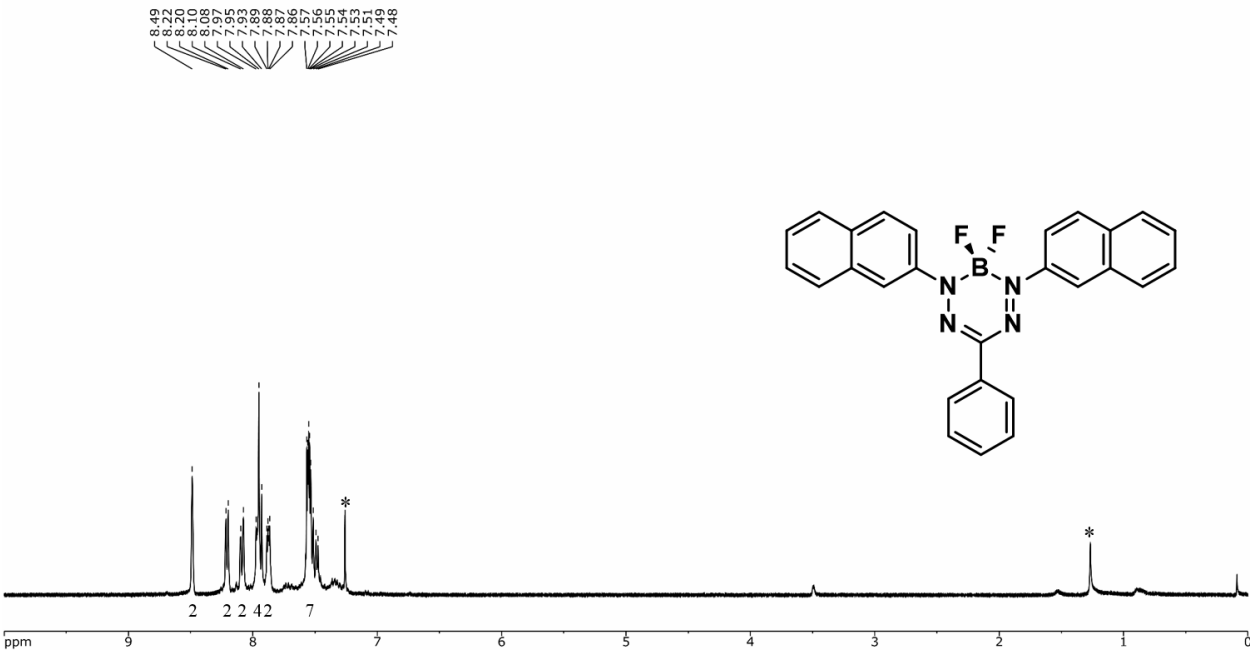

Figure S17. ^{1}H NMR spectrum of **7d** in $CDCl_3$. The asterisks denote residual solvent signals.

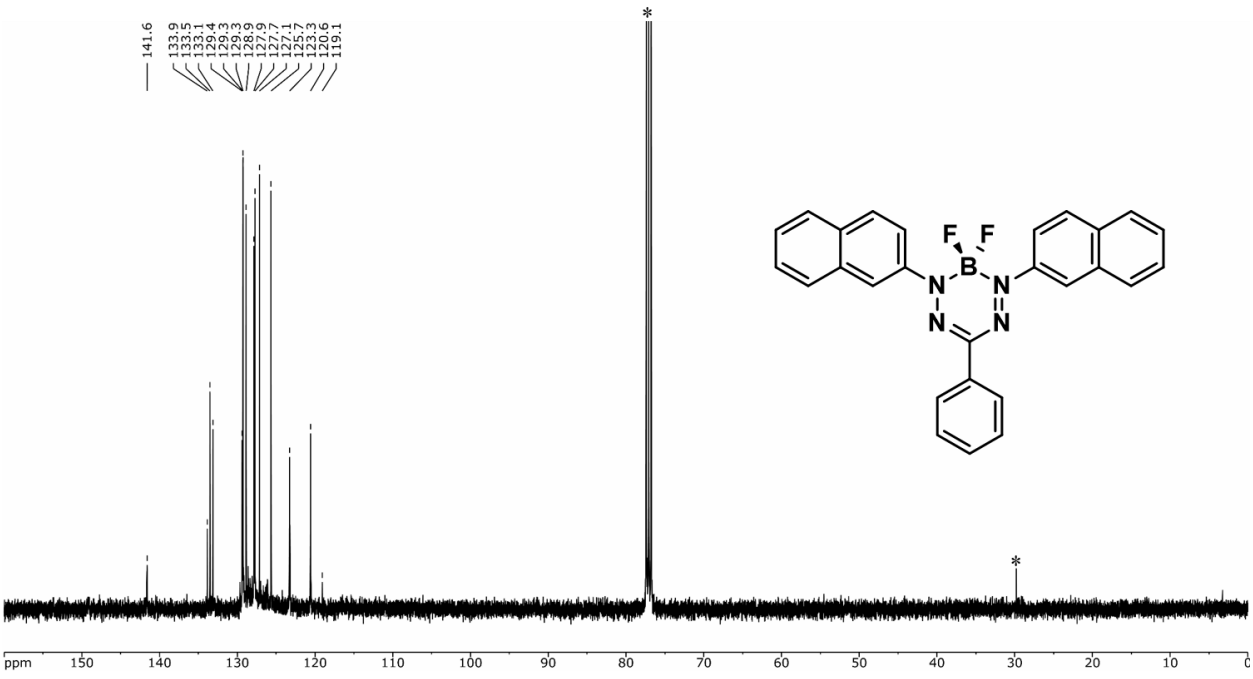

Figure S18. $^{13}C\{^{1}H\}$ NMR spectrum of **7d** in $CDCl_3$. The asterisk denotes $CDCl_3$ solvent signal.

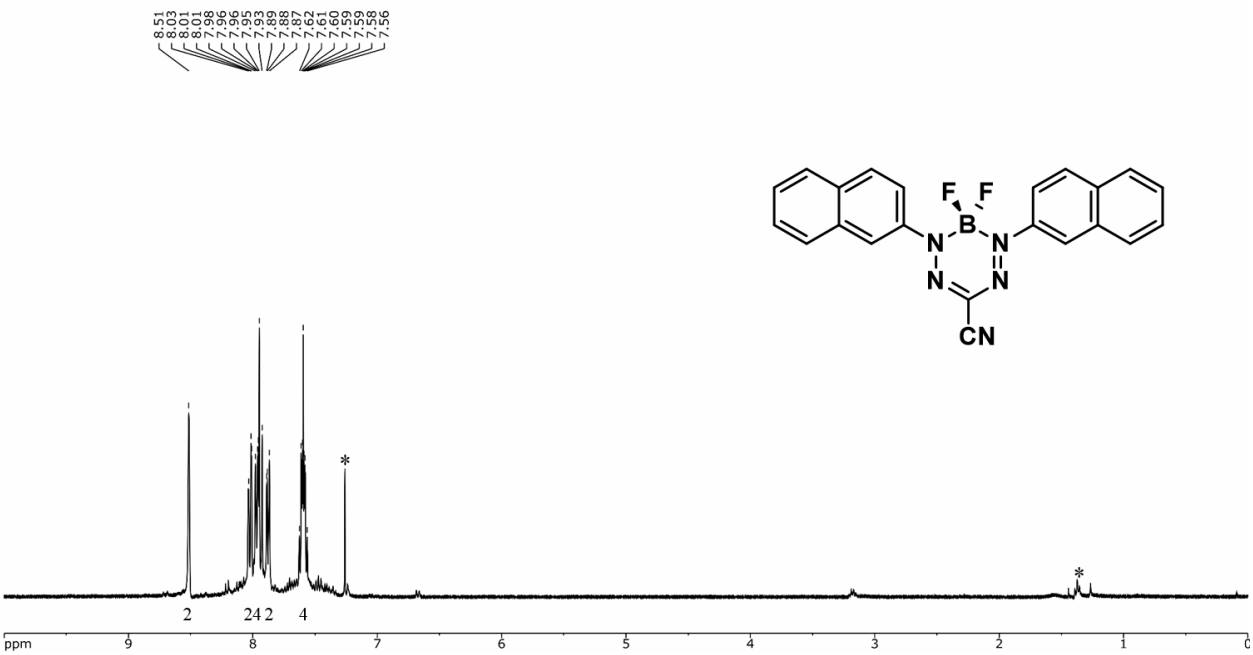

Figure S19. ^{1}H NMR spectrum of **7f** in $CDCl_3$. The asterisk denotes residual solvent signals.

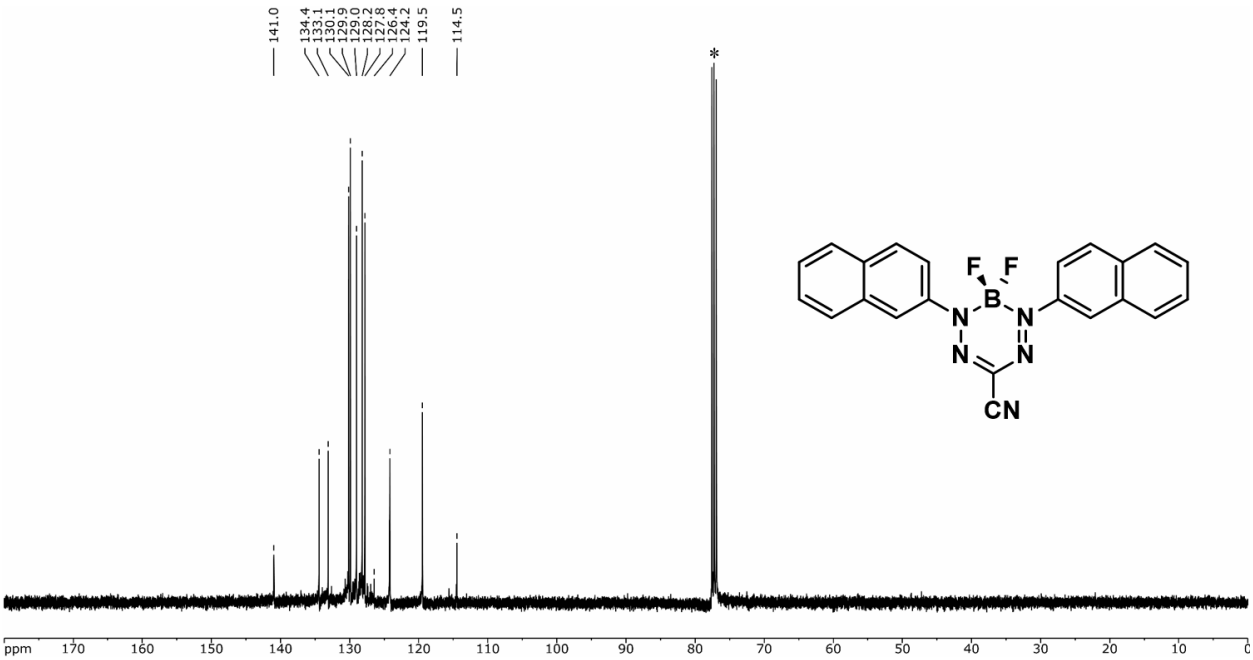

Figure S20. $^{13}C\{^{1}H\}$ NMR spectrum of **7f** in $CDCl_3$. The asterisk denotes $CDCl_3$ solvent signal.

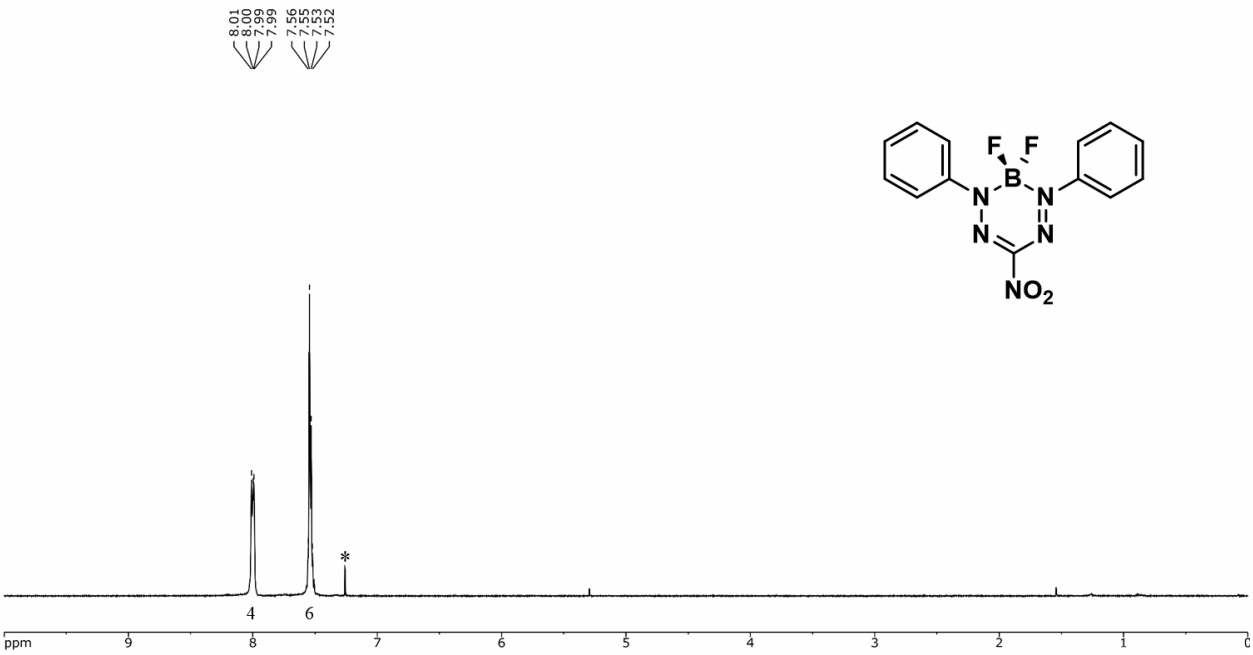

Figure S21. ^{1}H NMR spectrum of **7g** in $CDCl_3$. The asterisk denotes residual solvent signal.

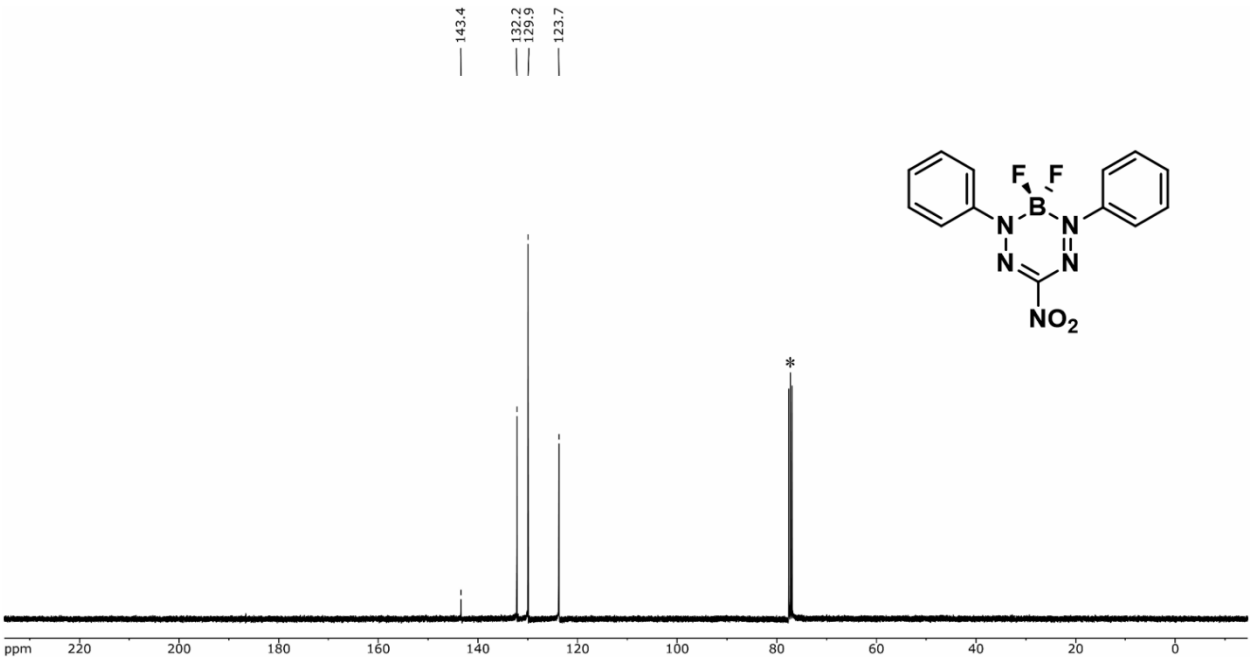

Figure S22. $^{13}C\{^{1}H\}$ NMR spectrum of **7g** in $CDCl_3$. The asterisk denotes $CDCl_3$ solvent signal.

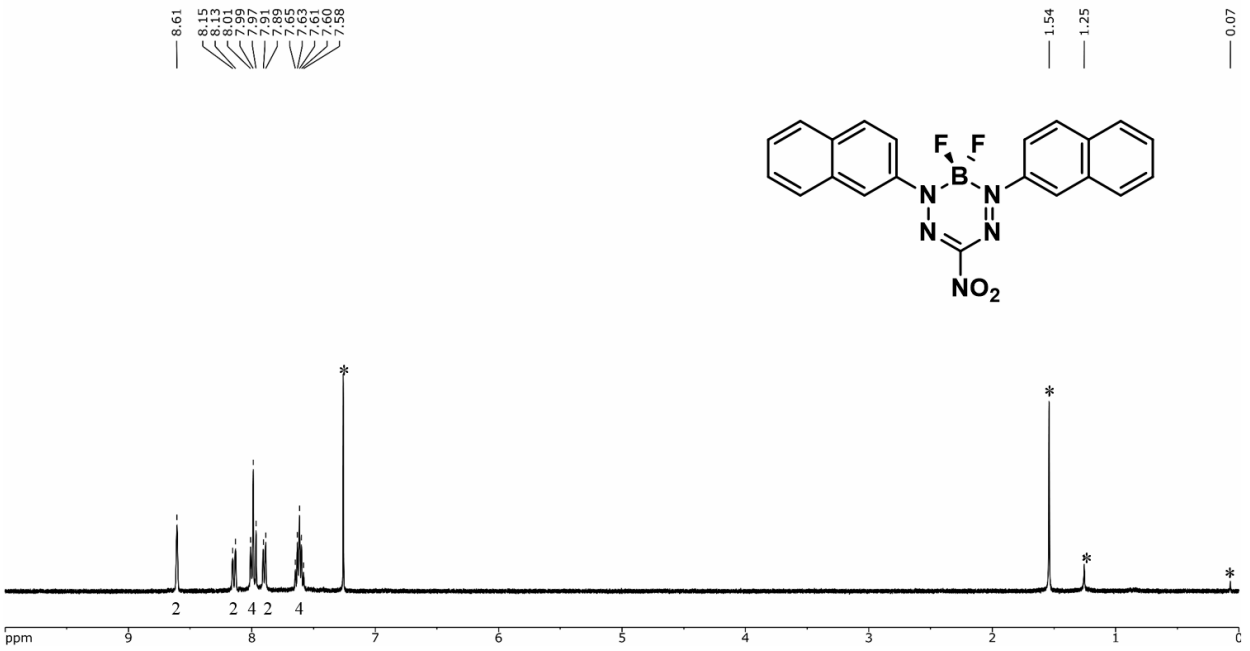

Figure S23. ^{1}H NMR spectrum of **7h** in $CDCl_3$. The asterisks denote residual solvent/grease signals.

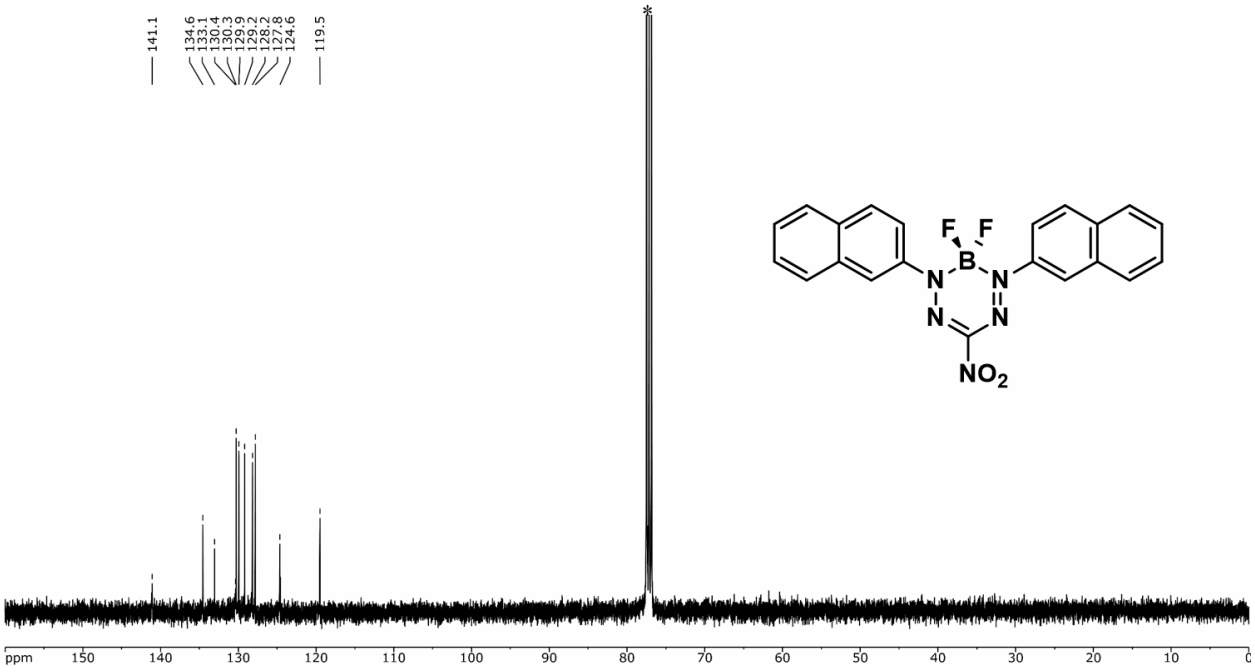

Figure S24. $^{13}C\{^{1}H\}$ NMR spectrum of **7h** in $CDCl_3$. The asterisk denotes $CDCl_3$ solvent signal.

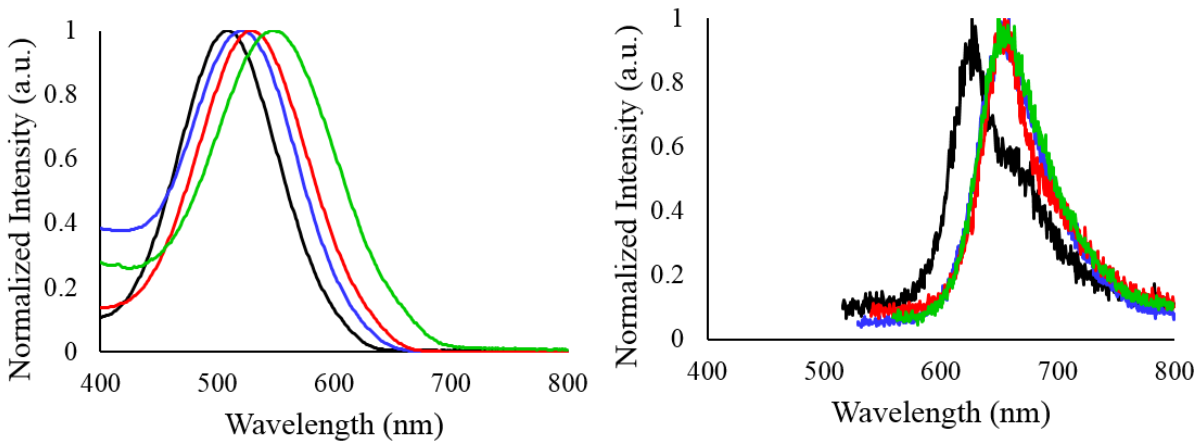

Figure S25. UV-vis absorption spectra (left) and emission spectra (right) of **7a** (black, Ar_1 = Ar_5 = R_3 = Ph), **7b** (blue, Ar_1 = Ar_5 = Ph, R_3 = Np), **7c** (red, Ar_1 = R_3 = Ph, Ar_5 = Np) and **7d** (green, Ar_1 = Ar_5 = Np, R_3 = Ph) recorded for 10^{-5} M degassed tetrahydrofuran solutions.

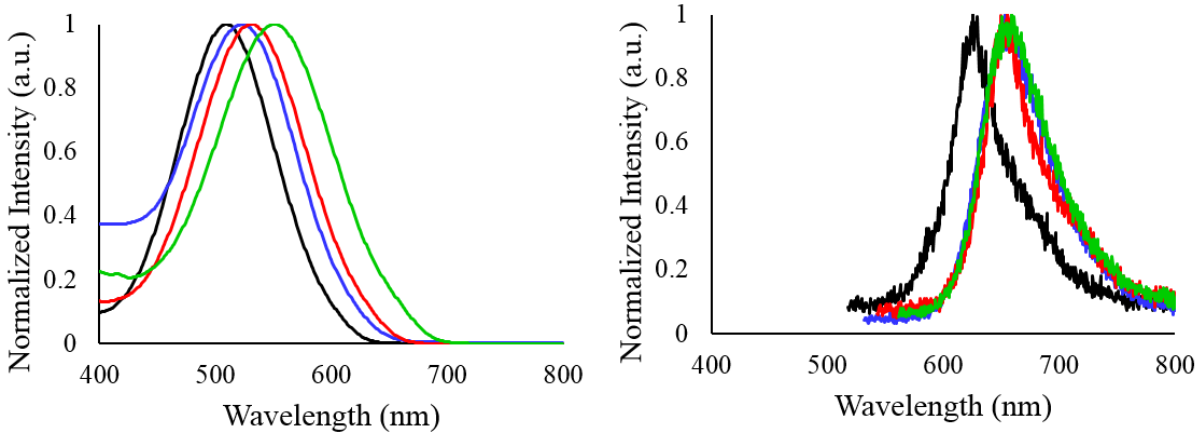

Figure S26. UV-vis absorption spectra (left) and emission spectra (right) of **7a** (black, Ar_1 = Ar_5 = R_3 = Ph), **7b** (blue, Ar_1 = Ar_5 = Ph, R_3 = Np), **7c** (red, Ar_1 = R_3 = Ph, Ar_5 = Np) and **7d** (green, Ar_1 = Ar_5 = Np, R_3 = Ph) recorded for 10^{-5} M degassed dichloromethane solutions.

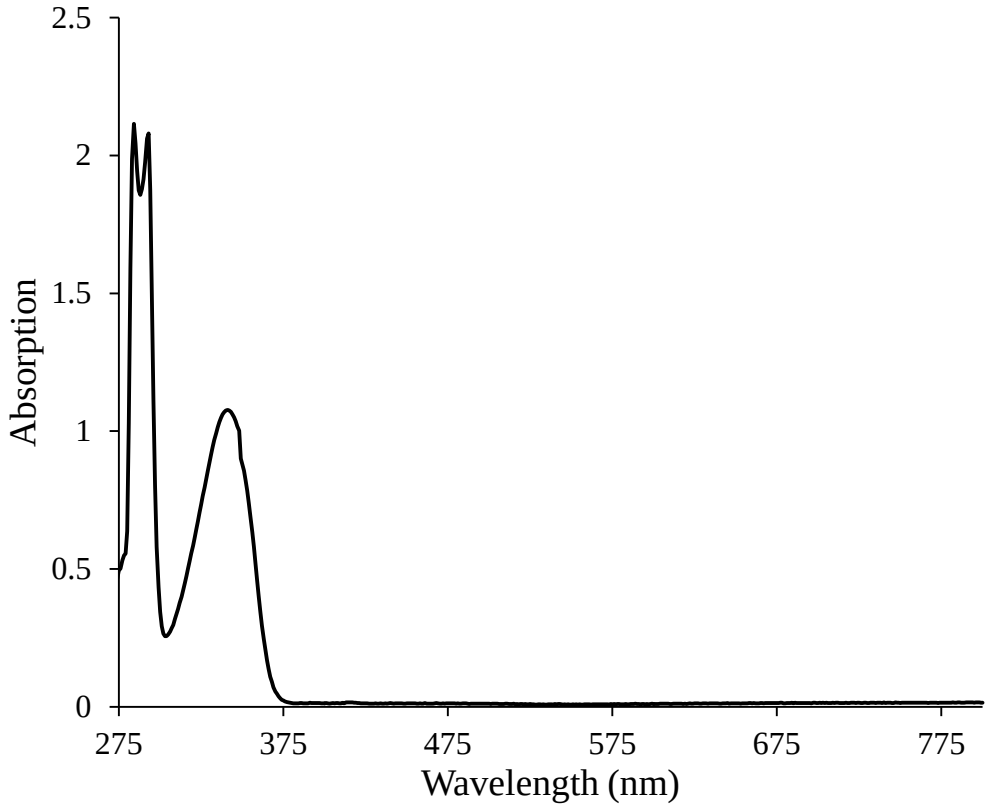

Figure S27. UV-vis absorption spectra of 2-naphthylamine in toluene.

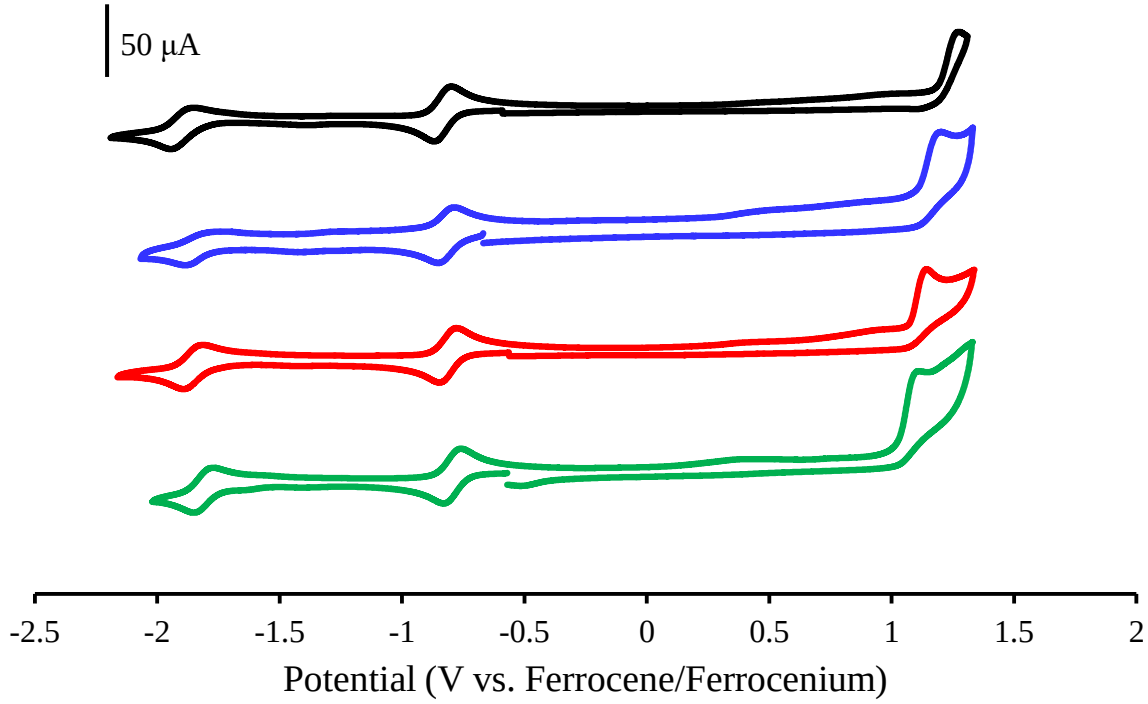

Figure S28. Cyclic voltammograms of **7a** (black, Ar_1 = Ar_5 = R_3 = Ph), **7b** (blue, Ar_1 = Ar_5 = Ph, R_3 = Np), **7c** (red, Ar_1 = R_3 = Ph, Ar_5 = Np) and **7d** (green, Ar_1 = Ar_5 = Np, R_3 = Ph) recorded at 100 mV s^{-1} in 1 mM acetonitrile solutions containing 0.1 M tetrabutylammonium hexafluorophosphate as supporting electrolyte.

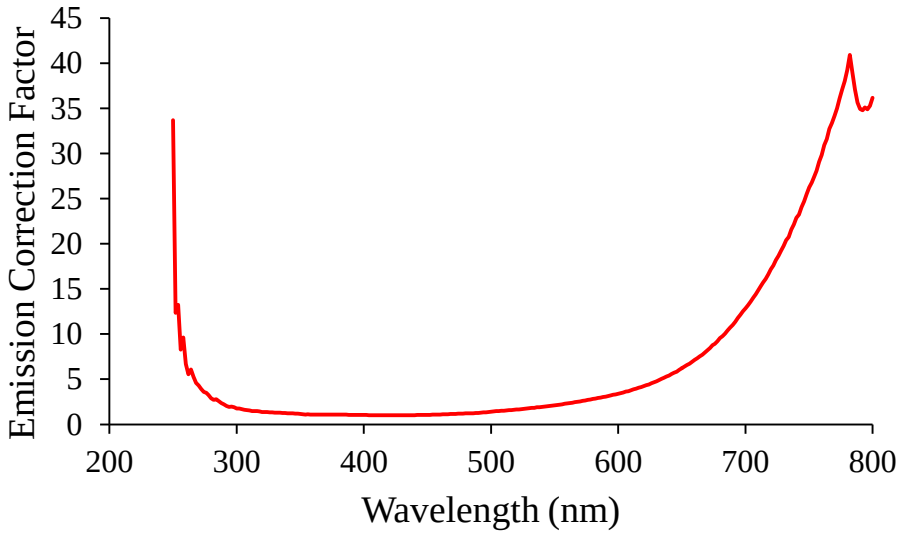

Figure S29. Wavelength-dependent emission correction provided by Photon Technology International.

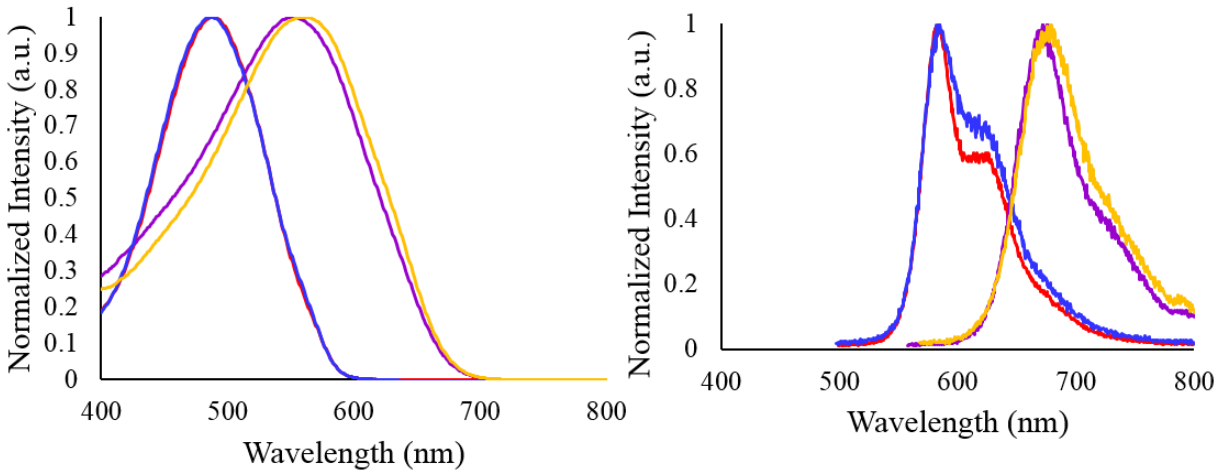

Figure S30. UV-vis absorption spectra (left) and emission spectra (right) of **7e** (red, $Ar_1 = Ar_5 =$ Ph, $R_3 =$ CN), **7f** (purple, $Ar_1 = Ar_5 =$ Np, $R_3 =$ CN), **7g** (blue, $Ar_1 = Ar_5 =$ Ph, $R_3 = NO_2$) and **7h** (orange, $Ar_1 = Ar_5 =$ Np, $R_3 = NO_2$) recorded for 10^{-5} M degassed tetrahydrofuran solutions.

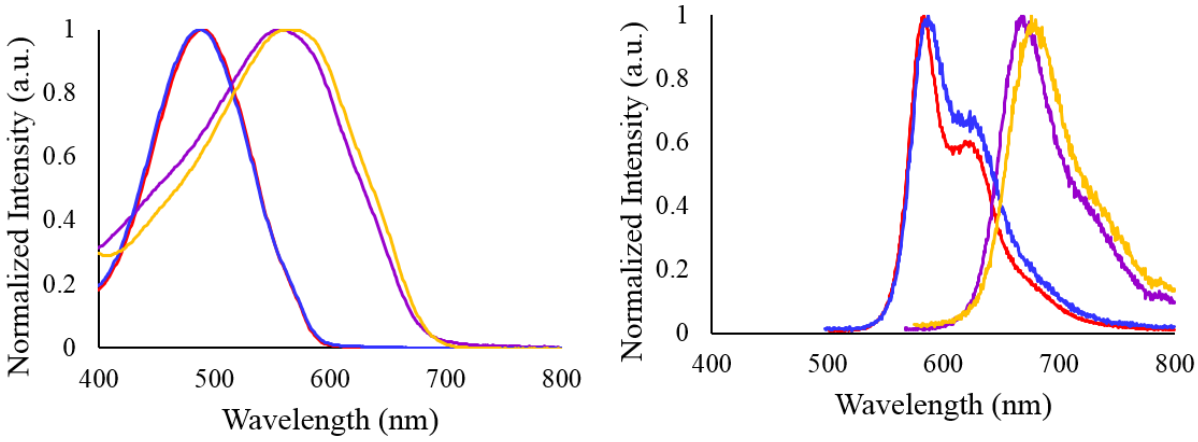

Figure S31. UV-vis absorption spectra (left) and emission spectra (right) of **7e** (red, $Ar_1 = Ar_5 =$ Ph, $R_3 =$ CN), **7f** (purple, $Ar_1 = Ar_5 =$ Np, $R_3 =$ CN), **7g** (blue, $Ar_1 = Ar_5 =$ Ph, $R_3 = NO_2$) and **7h** (orange, $Ar_1 = Ar_5 =$ Np, $R_3 = NO_2$) recorded for 10^{-5} M degassed dichloromethane solutions.

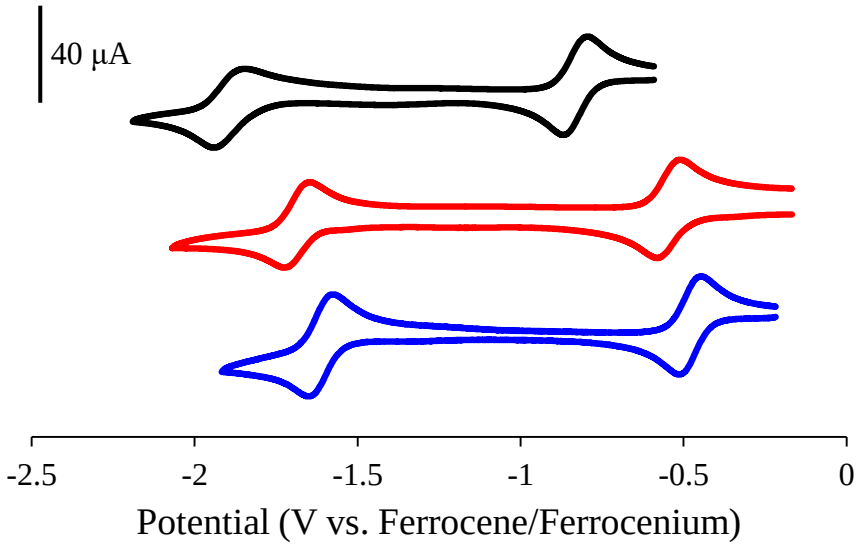

Figure S32. Cyclic voltammograms of **7a** (black, Ar_1 = Ar_5 = R_3 = Ph), **7e** (red, Ar_1 = Ar_5 = Ph, R_3 = CN) and **7g** (blue, Ar_1 = Ar_5 = Ph, R_3 = NO_2) recorded at 100 mV s^{-1} in 1 mM acetonitrile solutions containing 0.1 M tetrabutylammonium hexafluorophosphate as supporting electrolyte.

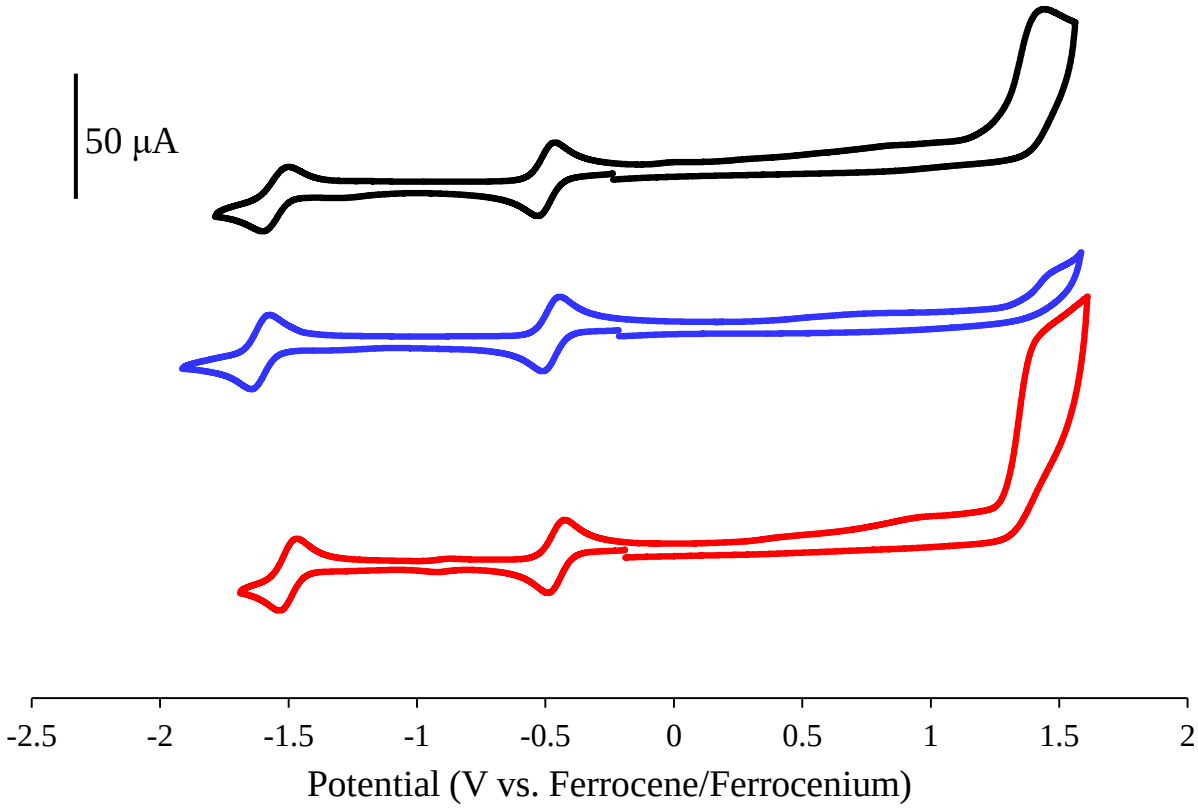

Figure S33. Cyclic voltammograms of **7f** (black, Ar_1 = Ar_5 = Np, R_3 = CN), **7g** (blue, Ar_1 = Ar_5 = Ph, R_3 = NO_2) and **7h** (red, Ar_1 = Ar_5 = Np, R_3 = NO_2) recorded at 100 mV s^{-1} in 1 mM acetonitrile solutions containing 0.1 M tetrabutylammonium hexafluorophosphate as supporting electrolyte

Calculated M06/6-311+G* structures of 7a, 7e and 7g in vacuum. All coordinates are in Å.

```
# M06/6-311+G* Int(Grid=UltraFine)

7a (R3 = Ph): Optimized M06/6-311+G* geometry (Cs), vacuum

0,1
C    -2.299578    0.585313    2.853536
C    -1.175665   -0.108575    2.411379
C    -0.668154   -1.174345    3.150842
C    -1.284588   -1.541730    4.333801
C    -2.404327   -0.851922    4.782527
C    -2.905976    0.209619    4.041017
N    -0.529006    0.292890    1.212974
B    -1.270421    0.958175    0.000000
F    -1.029154    2.312271    0.000000
N     0.745997    0.098380    1.175418
C     1.377226    0.181856    0.000000
C     2.849568    0.124243    0.000000
N     0.745997    0.098380   -1.175418
N    -0.529006    0.292890   -1.212974
C    -1.175665   -0.108575   -2.411379
C    -0.668154   -1.174345   -3.150842
C    -1.284588   -1.541730   -4.333801
C    -2.404327   -0.851922   -4.782527
C    -2.905976    0.209619   -4.041017
C    -2.299578    0.585313   -2.853536
F    -2.600368    0.644975    0.000000
H     0.204047   -1.707898   -2.784313
H    -0.892865   -2.378594   -4.907002
H    -2.888756   -1.144453   -5.711072
H    -3.777678    0.756474   -4.391756
H    -2.683402    1.422223   -2.278601
H     0.204047   -1.707898    2.784313
H    -0.892865   -2.378594    4.907002
H    -2.888756   -1.144453    5.711072
H    -3.777678    0.756474    4.391756
H    -2.683402    1.422223    2.278601
C     3.557768    0.101448   -1.201996
C     4.942106    0.038477   -1.199565
C     5.640459    0.003660    0.000000
C     4.942106    0.038477    1.199565
C     3.557768    0.101448    1.201996
H     3.013165    0.132890   -2.141827
H     5.480630    0.019967   -2.144471
H     6.727104   -0.043057    0.000000
H     5.480630    0.019967    2.144471
H     3.013165    0.132890    2.141827
```

```
--link1--
# M06/6-311+G* Int(Grid=UltraFine)

7e (R3 = CN): Optimized M06/6-311+G* geometry (Cs), vacuum

0,1
C     2.184147    0.281273    0.000000
N     1.592054    0.178650    1.193952
N     0.310659    0.227134    1.237759
B    -0.549547    0.698134    0.000000
F    -1.767671    0.086222    0.000000
N     0.310659    0.227134   -1.237759
N     1.592054    0.178650   -1.193952
F    -0.621312    2.069365    0.000000
C    -0.276053   -0.106306   -2.489581
C     3.614908    0.305524    0.000000
C    -0.276053   -0.106306    2.489581
N     4.766829    0.336450    0.000000
C     0.380141   -0.980914   -3.352634
C    -0.184198   -1.277993   -4.579801
C    -1.396999   -0.707861   -4.948618
C    -2.045561    0.162932   -4.083236
C    -1.493941    0.466078   -2.849707
H     1.325718   -1.421122   -3.050307
H     0.323173   -1.965514   -5.251801
H    -1.838958   -0.945645   -5.913137
H    -2.990577    0.616148   -4.371271
H    -1.995460    1.156584   -2.179414
C     0.380141   -0.980914    3.352634
C    -0.184198   -1.277993    4.579801
C    -1.396999   -0.707861    4.948618
C    -2.045561    0.162932    4.083236
C    -1.493941    0.466078    2.849707
H     1.325718   -1.421122    3.050307
H     0.323173   -1.965514    5.251801
H    -1.838958   -0.945645    5.913137
H    -2.990577    0.616148    4.371271
H    -1.995460    1.156584    2.179414
```

```
--link1--
# M06/6-311+G* Int(Grid=UltraFine)

7g (R3 = NO2): Optimized M06/6-311+G* geometry (Cs), vacuum

0,1
C    -1.728116    0.458177    2.847695
C    -0.508151   -0.115266    2.495884
C     0.152265   -0.974679    3.371506
C    -0.412065   -1.257196    4.601737
C    -1.628077   -0.687641    4.961672
C    -2.279483    0.169123    4.084700
N     0.078292    0.204595    1.240653
B    -0.775539    0.692758    0.000000
F    -0.819486    2.063567    0.000000
N     1.357319    0.123670    1.188209
C     1.925597    0.225301    0.000000
N     3.408092    0.213485    0.000000
N     1.357319    0.123670   -1.188209
N     0.078292    0.204595   -1.240653
C    -0.508151   -0.115266   -2.495884
C     0.152265   -0.974679   -3.371506
C    -0.412065   -1.257196   -4.601737
C    -1.628077   -0.687641   -4.961672
C    -2.279483    0.169123   -4.084700
C    -1.728116    0.458177   -2.847695
F    -2.002605    0.100989    0.000000
H     1.102650   -1.410422   -3.078049
H     0.098722   -1.931692   -5.284165
H    -2.069688   -0.914306   -5.929015
H    -3.226271    0.622642   -4.366210
H    -2.232219    1.138191   -2.168881
H     1.102650   -1.410422    3.078049
H     0.098722   -1.931692    5.284165
H    -2.069688   -0.914306    5.929015
H    -3.226271    0.622642    4.366210
H    -2.232219    1.138191    2.168881
O     3.954054    0.218392   -1.078741
O     3.954054    0.218392    1.078741
```

Calculated M06/6-311+G* structures of 7a, 7e and 7g in toluene solution. All coordinates are in Å.

```
--link1--
# M06/6-311+G* Int(Grid=UltraFine)SCRF=(PCM,Solvent=Toluene)

7a (R3 = Ph): Optimized M06/6-311+G* geometry (Cs), toluene solution

0,1
C    -0.611350   -2.279560    2.867417
C     0.104011   -1.179417    2.400459
C     1.206309   -0.701602    3.105236
C     1.589108   -1.324593    4.280354
C     0.877827   -2.420599    4.754425
C    -0.220441   -2.892768    4.046850
N    -0.311587   -0.524373    1.210790
B    -0.985853   -1.253685    0.000000
F    -2.341242   -0.992310    0.000000
N    -0.106454    0.749541    1.174641
C    -0.189131    1.382462    0.000000
C    -0.123721    2.854518    0.000000
N    -0.106454    0.749541   -1.174641
N    -0.311587   -0.524373   -1.210790
C     0.104011   -1.179417   -2.400459
C     1.206309   -0.701602   -3.105236
C     1.589108   -1.324593   -4.280354
C     0.877827   -2.420599   -4.754425
C    -0.220441   -2.892768   -4.046850
C    -0.611350   -2.279560   -2.867417
F    -0.700175   -2.591220    0.000000
H     1.757648    0.150682   -2.718579
H     2.454186   -0.957127   -4.826777
H     1.182164   -2.909949   -5.676411
H    -0.783767   -3.745034   -4.418228
H    -1.478149   -2.638472   -2.320971
H     1.757648    0.150682    2.718579
H     2.454186   -0.957127    4.826777
H     1.182164   -2.909949    5.676411
H    -0.783767   -3.745034    4.418228
H    -1.478149   -2.638472    2.320971
C    -0.096846    3.562675   -1.202275
C    -0.025124    4.946992   -1.199985
C     0.014372    5.645258    0.000000
C    -0.025124    4.946992    1.199985
C    -0.096846    3.562675    1.202275
H    -0.131411    3.019430   -2.142747
H    -0.003057    5.485176   -2.144886
H     0.068311    6.731474    0.000000
H    -0.003057    5.485176    2.144886
H    -0.131411    3.019430    2.142747
```

```
--link1--
# M06/6-311+G* Int(Grid=UltraFine)SCRF=(PCM,Solvent=Toluene)

7e (R3 = CN): Optimized M06/6-311+G* geometry (Cs), toluene solution

0,1
C     2.186655    0.286978    0.000000
N     1.595515    0.184729    1.194429
N     0.314638    0.242583    1.236854
B    -0.535905    0.726978    0.000000
F    -1.767225    0.140288    0.000000
N     0.314638    0.242583   -1.236854
N     1.595515    0.184729   -1.194429
F    -0.584603    2.102405    0.000000
C    -0.278213   -0.104836   -2.482029
C     3.617127    0.302617    0.000000
C    -0.278213   -0.104836    2.482029
N     4.769362    0.327999    0.000000
C     0.352002   -1.025943   -3.315512
C    -0.216635   -1.338035   -4.537350
C    -1.407390   -0.736394   -4.928442
C    -2.030670    0.180259   -4.091368
C    -1.474626    0.498448   -2.863456
H     1.277777   -1.493989   -2.994080
H     0.268703   -2.062159   -5.186506
H    -1.852803   -0.985815   -5.888262
H    -2.957745    0.657477   -4.397742
H    -1.954943    1.225967   -2.216822
C     0.352002   -1.025943    3.315512
C    -0.216635   -1.338035    4.537350
C    -1.407390   -0.736394    4.928442
C    -2.030670    0.180259    4.091368
C    -1.474626    0.498448    2.863456
H     1.277777   -1.493989    2.994080
H     0.268703   -2.062159    5.186506
H    -1.852803   -0.985815    5.888262
H    -2.957745    0.657477    4.397742
H    -1.954943    1.225967    2.216822
```

```
--link1--
# M06/6-311+G* Int(Grid=UltraFine)SCRF=(PCM,Solvent=Toluene)

7g (R3 = NO2): Optimized M06/6-311+G* geometry (Cs), toluene solution

0,1
C    -1.702774    0.502704    2.861272
C    -0.512572   -0.114662    2.482338
C     0.107934   -1.040583    3.318257
C    -0.465476   -1.344361    4.539549
C    -1.650732   -0.729698    4.927865
C    -2.263486    0.192252    4.088952
N     0.085660    0.225908    1.238492
B    -0.750350    0.743507    0.000000
F    -0.743785    2.117743    0.000000
N     1.363411    0.127875    1.188524
C     1.932407    0.230393    0.000000
N     3.409584    0.207030    0.000000
N     1.363411    0.127875   -1.188524
N     0.085660    0.225908   -1.238492
C    -0.512572   -0.114662   -2.482338
C     0.107934   -1.040583   -3.318257
C    -0.465476   -1.344361   -4.539549
C    -1.650732   -0.729698   -4.927865
C    -2.263486    0.192252   -4.088952
C    -1.702774    0.502704   -2.861272
F    -2.000060    0.200581    0.000000
H     1.030993   -1.516047   -3.000226
H     0.012225   -2.071241   -5.191153
H    -2.099771   -0.972866   -5.887574
H    -3.185604    0.679852   -4.393724
H    -2.174852    1.234515   -2.213576
H     1.030993   -1.516047    3.000226
H     0.012225   -2.071241    5.191153
H    -2.099771   -0.972866    5.887574
H    -3.185604    0.679852    4.393724
H    -2.174852    1.234515    2.213576
O     3.961070    0.208547   -1.077611
O     3.961070    0.208547    1.077611
```